Physics – Uspekhi **44** (5) 515 – 539 (2001)

REVIEWS OF TOPICAL PROBLEMS PACS numbers: 74.20.Mn, **74.72. – h**, **74.25. – q**, 74.25.Jb

Pseudogap in high-temperature superconductors

M V Sadovskiĭ

DOI: 10.1070/PU2001v044n05ABEH000902

Contents

Abstract. The paper reviews the basic experimental facts and a number of theoretical models relevant to the understanding of the pseudogap state in high-temperature superconductors. The state is observed in the region of less-than-optimal current-carrier concentrations in the HTSC cuprate phase diagram and manifests itself as various anomalies in the electronic properties, presumably due to the antiferromagnetic short-range-order fluctuations that occur as the antiferromagnetic region of the phase diagram is approached. The interaction of current carriers with these fluctuations leads to an anisotropic transformation of the electron spectrum and causes the system to behave as a non-Fermi liquid in certain regions of the Fermi surface. Simple theoretical models for describing the basic properties of the pseudogap state, in particular renormalization-induced anomalies in the superconducting state, are discussed.

1. Introduction

The study of high-temperature (or high-T_c) superconductivity (HTSC) in copper oxides remains one of the central avenues of research in the physics of the condensed state. Despite enormous efforts of both experimenters and theoreticians, the nature of this phenomenon remains unclear. It is a well-known fact that the main difficulties here are related to the very unusual properties of these systems in the normal (nonsuperconducting) state, and without a clear understanding of the nature of these properties there is little hope for completely elucidating the microscopic mechanism of high-T_c superconductivity. In recent years one of the main aspects of high-T_c superconductor physics has been the study of the anomalies of what is known as the pseudogap state [1], which is observed in the region of the phase diagram corresponding to charge-carrier concentrations lower than optimal one (i.e. the concentration corresponding to the maximum temperature of the superconducting transition, T_c); it is usually called the 'underdoped' region. In this region there are many anomalies of the electronic properties in both the normal and the superconducting state, which are related to the drop in the single-particle density of states and to the anisotropic transformation of the charge-carrier spectral density. The understanding of the nature and properties of the pseudogap state is the central problem of any approach to the description of the complex phase diagram of HTSC systems. Hundreds of experimental and theoretical papers have been devoted to this problem [1].

The goal of the present review is to present the main experimental facts pertaining to the observations of the pseudogap state in underdoped high-T_c cuprates and to discuss a number of simple theoretical models of this state. The review is not exhaustive in either describing the experimental data or giving the full theoretical picture. The experimental data are presented fairly briefly, since the literature already has a number of good reviews [2 – 6]

M V Sadovskiĭ Institute of Electrophysics, Ural Branch of the Russian Academy of Sciences
ul. Amundsena 106, 620016 Ekaterinburg, Russian Federation
Tel. (7-3432) 67 87 86. Fax (7-3432) 67 87 94
E-mail: sadovski@iep.uran.ru

Received 27 November 2000, revised 8 February 2001
Uspekhi Fizicheskikh Nauk **171** (5) 539 – 564 (2001)
Translated by E Yankovsky; edited by A V Getling

[1] Suffice it to say that the well-known E-archive of preprints, cond-mat, contains more than 600 papers devoted, in one way or another, to the physics of the pseudogap sate. At the major conference on superconductivity held in Houston, M^2S – HTSC-VI (February 2000), four section meetings were devoted to this problem — more than to any other problem of HTSC physics.

devoted to these problems in one way or another. The theoretical part is also fairly subjective and, to a large extent, reflects the author's viewpoint. There are two basic theoretical scenarios for explaining the pseudogap anomalies of HTSC systems. The first one is based on the model in which Cooper pairs are formed above the transition temperature [7–10], with the subsequent establishment of their phase coherence at $T < T_c$. The second scenario assumes that the pseudogap state emerges due to 'dielectric' type, short-range-order fluctuations, which are present in the region of underdoped compositions in the phase diagram. The most popular picture here is that of antiferromagnetic (AFM) fluctuations [11–15], although one cannot exclude that fluctuations of charge-density waves (CDW), structural distortions, or phase separation on a microscopic scale can play a similar role. I believe that many experiments conducted in recent years speak in favor (fairly persuasively) of the second scenario. Hence in our theoretical discussion we will limit ourselves to relevant models, giving a quite full description of the work of the present author and his collaborators, and also of the work of other researchers whose main ideas and approaches are in the same vein. Accordingly, in the most part of the review we will deal with the model of antiferromagnetic fluctuations, although its validity cannot be thought of as fully corroborated.

Neither can we claim that the list of references is complete and, the more so, that it reflects priorities in this field. It is assumed that the reader will find the necessary literature from the papers in the list of references. The author would like to apologize to the numerous authors of papers not cited here — the aim was to make the list not too long.

2. Basic experimental facts

Typical variants of the phase diagram of HTSC cuprates are depicted in Fig. 1. Depending on the concentration of charge carriers (mainly holes), several phases and regions with anomalous physical properties can be observed in the high-conductivity CuO_2 plane. In the region of low hole concentrations all known HTSC cuprates are antiferromagnetic insulators. As the current-carrier concentration increases, the Néel temperature T_N rapidly drops from values of several hundred kelvins and vanishes at hole concentrations p lower or of order 0.05, with the system becoming a (poor) metal. A further increase in the hole concentration transforms the system into a superconductor, with the transition temperature increasing with the carrier concentration and going through a characteristic maximum at $p_0 \sim 0.15-0.17$ (optimum doping) and then decreasing and vanishing at $p \sim 0.25-0.30$, although in this (overdoped) region the metallic behavior is still quite evident. Here, at $p > p_0$ the metallic properties are fairly traditional (Fermi-liquid behavior), while at $p < p_0$ the system becomes an anomalous metal, whose behavior (as most researchers believe) cannot be described by the Fermi-liquid theory [2].

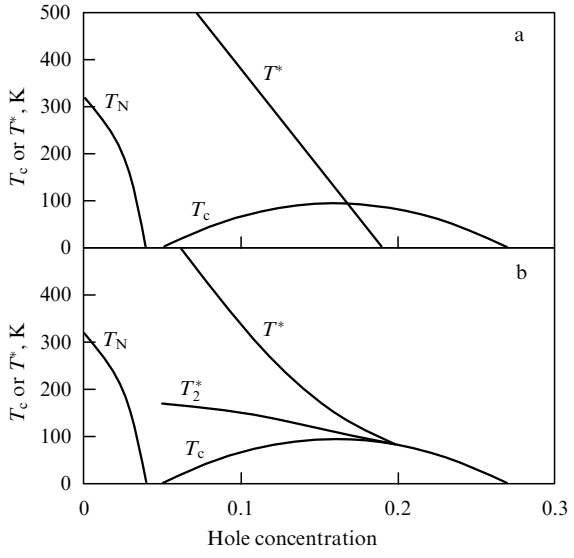

Figure 1. Variants of the phase diagram of high-T_c cuprates.

The anomalies of physical properties currently attributed to the formation of a pseudogap state are observed in the metallic phase at $p < p_0$ and at temperatures $T < T^*$, where T^* decreases from values of order T_N at $p \sim 0.05$ and vanish at a certain 'critical' carrier concentration p_c somewhat higher than p_0 (Fig. 1a). For instance, Tallon and Loram [6] stated that this happens at $p = p_c \approx 0.19$. According to some researchers (mostly adherents of the idea of the superconducting nature of the pseudogap), T^* merges with the line of the superconducting-transition temperature T_c near the optimum concentration p_0 (Fig. 1b). Below we will see that the majority of new experimental data most likely support the variant of the phase diagram depicted in Fig. 1a (for more details see Ref. [6]). Note that most researchers agree that T^* does not have the meaning of the temperature of a phase transition; rather, it simply defines a characteristic temperature scale below which pseudogap anomalies appear in the system. In this region of the phase diagram a system exhibits no features characteristic of phase transitions in the behavior of thermodynamic quantities [3]. The general idea is that all these anomalies, to put it simply, are related to the suppression (in the given region) of the density of states of single-particle excitations near the Fermi level, which is what the general concept of the pseudogap means [4]. Here T^* is simply proportional to the size of the pseudogap on the energy scale. Sometimes another characteristic temperature scale is specified, T_2^* (see Fig. 1b), which is related to the transition from a 'weak'- to a 'strong'-pseudogap regime [14]. The reasoning here is based on a change in the spin response of the system in the vicinity of this temperature. In the present review we almost never touch on the corresponding details.

Now let us turn to a detailed description of the most typical experimental manifestations of the corresponding anomalies in HTSC cuprates.

[2] Note that the problem of whether or not HTSC systems behave like Fermi liquids has become very involved due to the discussions of numerous researchers belonging to different schools and often using very different definitions of the idea of a Fermi liquid. In what follows we use the terminology adopted by the majority of researchers (although this majority is not cleary defined).

[3] However, it is only proper to note that recently Chakravarty et al. [16] proposed an opposite idea, namely, that the line of T^* in the phase diagram is directly linked to a 'hidden' symmetry breaking, strongly 'blurred' by the internal disorder.

[4] The idea of a pseudogap was first formulated by Mott in the qualitative theory of disordered (noncrystalline) semiconductors [17]. According to Mott, a pseudogap is a region of reduced electronic-state density within an energy interval corresponding to the forbidden band of an ideal crystal and is simply a 'recollection' about this band that is retained even under strong disordering (amorphization, melting, etc.).

2.1 Specific heat and tunneling

Let us consider data on the electronic contribution to the specific heat of HTSC cuprates. For metals this contribution is usually written as $C = \gamma(T)T$, so that in the normal state ($T > T_c$) we have $\gamma \sim N(0)$, where $N(0)$ is the density of states at the Fermi level. At $T = T_c$ there emerges a well-known anomaly related to a second-order phase transition, and the temperature dependence $\gamma(T)$ has a characteristic peak (discontinuity). As an example, Fig. 2 depicts typical experimental data for the $Y_{0.8}Ca_{0.2}Ba_2Cu_3O_{7-\delta}$ system at different values of δ [18]. In optimally doped and overdoped samples, the temperature dependence $\gamma(T)$ is practically a straight line parallel to the temperature axis over the entire region where $T > T_c$, while in underdoped samples there is a substantial lowering of $\gamma(T)$ in the temperature range $T < 150-200$ K. This fact directly indicates that the density of electronic states at the Fermi level drops and that a pseudogap forms when $T < T^*$.

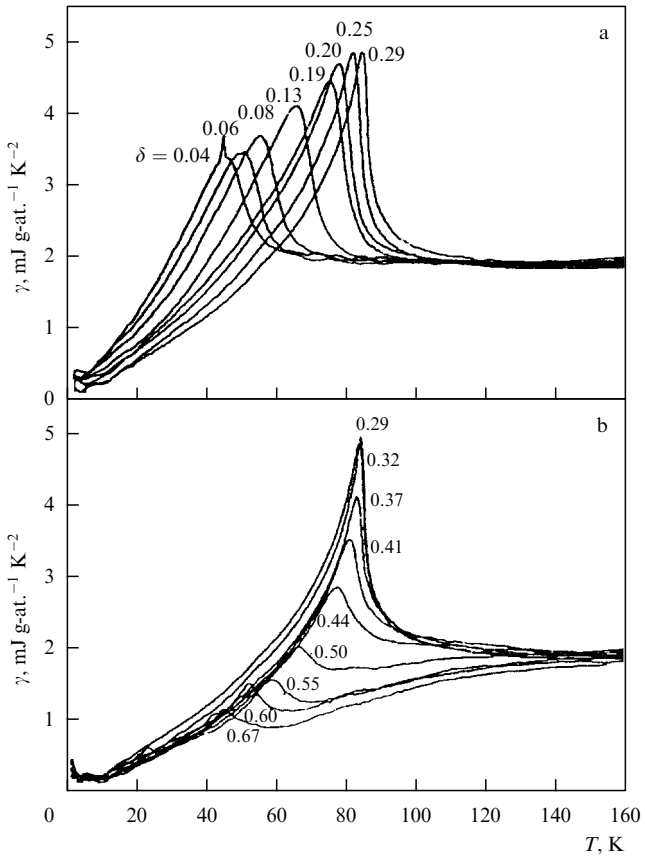

Figure 2. Electronic specific-heat coefficient γ in (a) overdoped and (b) underdoped $Y_{0.8}Ca_{0.2}Ba_2Cu_3O_{7-\delta}$ [18].

We also note that near the transition temperature T_c the size of the specific-heat discontinuity decreases substantially with the transition to the region of underdoped compositions. A more thorough analysis done by Tallon and Loram [6] shows that the corresponding discontinuity $\Delta\gamma_c$ begins to rapidly diminish starting with the 'critical' carrier concentration $p_c \approx 0.19$, which is considered the moment of emergence of a pseudogap in the electron spectrum.

Combining the data on the specific heat with the more or less standard ideas of the BCS theory, we can attempt to estimate the width of the energy gap in the electron spectrum and its temperature dependence. Figure 3 depicts the data on

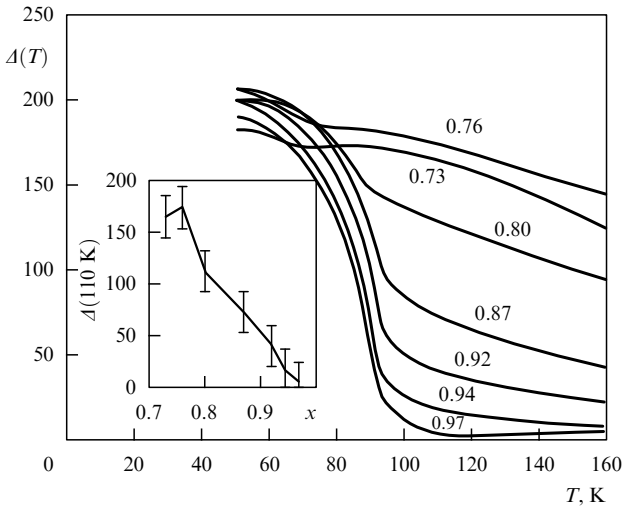

Figure 3. Temperature dependence of the energy gap for different compositions of $YBa_2Cu_3O_{6+x}$ determined from the specific-heat data of Loram et al. [19]. The numbers at the curves specify the corresponding values of x. The inset shows the data for the gap at $T = 110$ K.

the $YBa_2Cu_3O_{7-\delta}$ (YBCO) system gathered by Loram et al. [19]. Clearly, the energy gap in the spectrum estimated in this manner does not vanish at $T = T_c$ (as it should vanish in a standard superconductor) but instead extends itself into the region of higher temperatures, and the greater the underdoping the stronger the effect. Very often these data are naively interpreted as evidence for the existence of Cooper pairs at temperatures $T > T_c$.

The formation of a pseudogap in the density of states is clearly seen from experiments on single-particle tunneling. For instance, the frequently cited paper written by Renner et al. [20] describes tunneling experiments involving single crystals of $Bi_2Sr_2CaCu_2O_{8+\delta}$ (Bi-2212) with varying oxygen content. For underdoped samples the formation of a pseudogap in the density of states was clearly observed at temperatures much higher than T_c. Here the pseudogap smoothly evolved into a superconducting gap in the region $T < T_c$, which has also been frequently interpreted as direct evidence for the superconducting nature of the pseudogap. Traces of the existence of a pseudogap were also observed by the same researchers in slightly overdoped samples.

Usually, in discussing tunneling experiments involving HTSC cuprates, the question of the quality of the surfaces of the investigated samples is important. Hence of special interest are the recent investigations conducted by Krasnov et al. [21, 22]. They measured the intrinsic tunneling in mesa-structures [5] created on the surface of the same Bi-2212 system and were able to clearly demonstrate the existence of a superconducting gap, which vanishes at $T = T_c$, against the background of a smooth pseudogap, which exists even at higher temperatures. The relevant data are depicted in Fig. 4a. Clearly, typical features of the formation of a superconducting gap exist against the background of a smooth minimum of the density of states. What is especially important is that Krasnov et al. [22] have shown that the superconducting features of the tunnel characteristics are suppressed by an

[5] Mesa (Spanish 'table'), flat-topped tableland with one or more steep sides, common in the Colorado Plateau regions of the United States and Mexico (Mesa Central) (*Britannica CD97, 1997*).

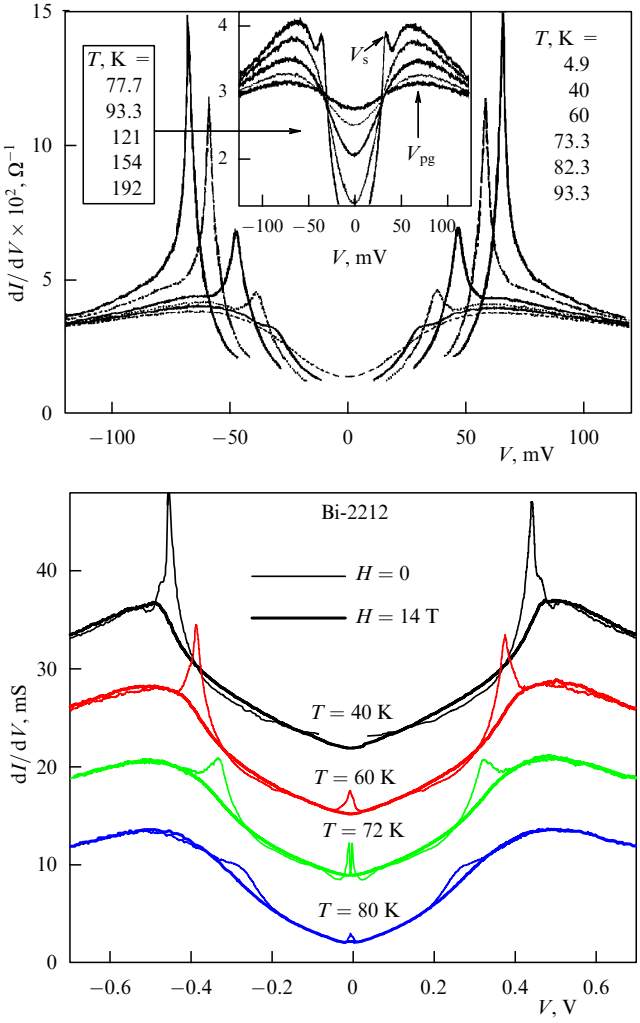

Figure 4. (a) Differential conductance of almost optimally doped Bi-2212 at different temperatures. The inset shows the results for high temperatures [21]. (b) Similar data in an external magnetic field $H = 0$ (light lines) and in a field $H = 14$ T (heavy lines) [22].

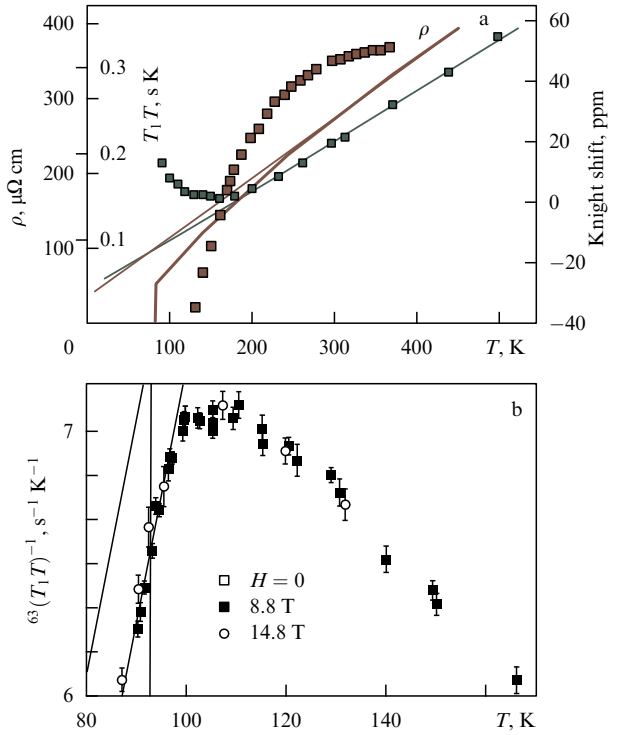

Figure 5. (a) Effect of pseudogap formation on the electrical resistivity, the Knight shift, and the NMR relaxation time in underdoped $YBa_2Cu_4O_8$. The changes in the temperature dependence in the region $T < 200-300$ K are attributed to pseudogap formation in the density of states [1]. (b) The NMR relaxation frequency $(TT_1)^{-1}$ of slightly underdoped $YBa_2Cu_3O_{7-\delta}$ in a strong magnetic field directed along the crystallographic c-axis [26]. The vertical line corresponds to T_c for zero field, and the slanted line gives an estimate for the shift in the data expected in the case of suppression of the pseudogap by a magnetic field; its position is determined by the observed shift in T_c.

external magnetic field, while the size of the pseudogap proves to be almost independent of the field strength, which points to its nonsuperconducting nature. The corresponding data are depicted in Fig. 4b.

2.2 NMR and kinetic properties

Pseudogap formation also manifests itself in the kinetic properties of HTSC systems in the normal state, the Knight shift, and the NMR relaxation time. In particular, a feature related to such formation is the change in the standard (for optimally doped compositions) linear temperature dependence of the electrical resistivity in the region $T < T^*$ for underdoped samples. The Knight shift in such samples proves to be temperature dependent: in the region $T < T^*$ there is a rapid drop in the value of this quantity. In underdoped samples the quantity $(TT_1)^{-1}$, where T_1 is the NMR spin–lattice relaxation time, behaves in a similar manner. The reader will recall that in common metals the Knight shift is proportional to $N(0)$, while $(TT_1)^{-1} \sim N^2(0)$ (Korringa behavior), and the electrical resistivity ρ is proportional to the scattering rate (the inverse of the mean free time) $\gamma \sim N(0)$. Hence it is natural that the significant decrease in all these quantities is related to the drop in the density of electronic states, $N(0)$, at the Fermi level [6]. Figure 5a, taken from Batlogg and Varma's paper [1], shows a summary of the relevant experimental data for underdoped samples of the $YBa_2Cu_4O_8$ system based on the papers of Bucher et al. [23], Yasuoka [24], and Alloul and Adrian [25]. Note that this interpretation is, of course, extremely simplified, especially when one is speaking of the temperature dependence of the corresponding quantities. For instance, in the case of electrical resistivity this dependence is largely determined by inelastic scattering, whose physics in HTSC systems still remains not completely understood. In particular, a decrease in the density of states (with the spectrum becoming partially dielectric) could lead to a corresponding increase in electrical resistivity.

Figure 5b depicts the experimental data of Gorny et al. [26], who measured $(TT_1)^{-1}$ on ^{63}Cu nuclei in slightly underdoped $YBa_2Cu_3O_{7-\delta}$ in a sufficiently strong magnetic field. Clearly, there is no magnetic-field dependence, which is a strong argument in favor of the nonsuperconducting nature of the pseudogap, since otherwise a magnetic field would substantially change the magnitude of the effect. Note that

[6] Historically speaking, the first data on the significant drop in the density of states in underdoped cuprates were gathered precisely in NMR experiments and in the magnetic scattering of neutrons. Hence the first term actively used was 'spin gap.' Later studies revealed similar effects related not only to the spin degrees of freedom, and so the term 'pseudogap' became generally accepted.

the strong influence of a magnetic field on the size of the Knight shift and the NMR relaxation frequency of ^{63}Cu was observed in slightly overdoped $TlSr_2CaCu_2O_{6.8}$, where it can be described fairly well in terms of the effect of suppression of superconducting fluctuations [27]. This fact is strong evidence in favor of the disappearance (at a certain lower carrier concentration) of the pseudogap of a nonsuperconducting nature (independent of the magnetic field) discussed above.

Note that in different experiments the temperature T^* below which anomalies associated with pseudogap formation emerge is somewhat different, depending on the quantity that is measured. However, in all cases there is a systematic dependence of T^* on the doping level, and this temperature vanishes when the carrier concentration is equal to or somewhat higher than the optimal doping level. This implies that T^* is not a clearly defined temperature (say, of a phase transition); it only determines the scale of the temperature (energy) below which these anomalies manifest themselves. One can attempt to determine the corresponding energy scale from experiments, say, by modeling the pseudogap by a V-like energy dependence (with a width E_g) of the density of states near the Fermi level (then $T^* = 0.4E_g$) [6]. Figure 6 depicts the consolidated data for the gap widths in YBCO found in this manner (from processing the results of different experiments) as a function of hole concentration [6]. Clearly, the pseudogap 'closes' at the critical value $p_c \approx 0.19$. We note once more that both the T^*-line in the phase diagram and the 'critical' concentration p_c have a fairly conventional meaning. Nevertheless, some researchers have attempted to interpret p_c as a 'quantum' critical point (QCP) of some sort [28].

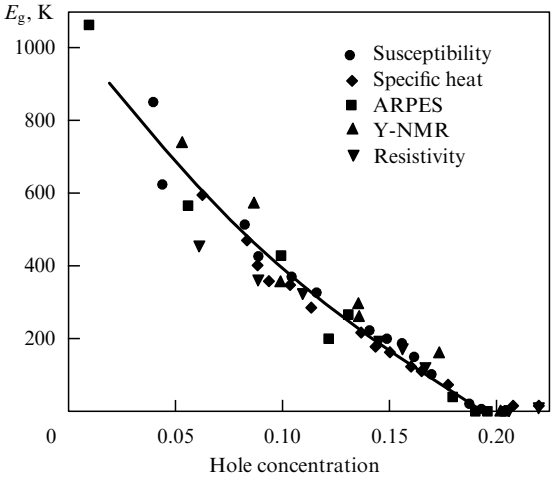

Figure 6. Dependence of the energy width E_g of the pseudogap in YBCO on the hole concentration p according to the data from different experiments [6].

2.3 Optical conductivity

Pseudogap formation in the region of underdoped compositions of HTSC cuprates also manifests itself very clearly in experiments measuring optical conductivity, both in the direction of the electric field vector along the high-conductivity CuO_2 plane and in the perpendicular direction along the tetragonal c-axis. The relevant data have been described fairly thoroughly by Timusk and Statt [2] and Puchkov et al. [29]. As a typical example, in Fig. 7a we depict the data of Startseva et al. [30] on optical conductivity in the CuO_2 plane of

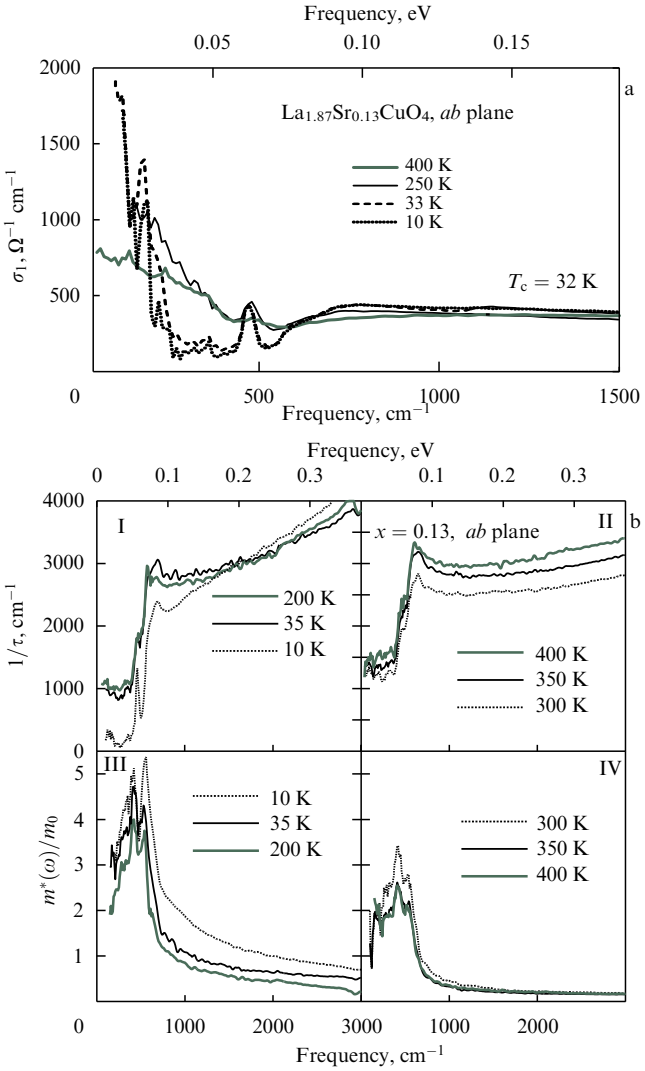

Figure 7. (a) Real part of the optical conductivity in the *ab* plane of $La_{1.87}Sr_{0.13}CuO_4$ at different temperatures T [30]. (b) Generalized scattering rate and effective mass as functions of the external-field frequency obtained through processing the optical data for the same system by the extended Drude formula [30]: I and III, for temperatures below 250 K, where a linear increase in $1/\tau$ with frequency is observed in the region $\omega > 700\ \text{cm}^{-1}$; II and IV, at higher temperatures, where a linear increase in $1/\tau$ is almost unnoticeable.\

underdoped $La_{1.87}Sr_{0.13}CuO_4$. Characteristic features of these data are the presence of a narrow Drude peak in the frequency range $\omega < 250\ \text{cm}^{-1}$ and the appearance of a 'pseudogap dip' in the interval from 250 to 700 cm^{-1} with a diffuse maximum in the vicinity of $\omega \sim 800\ \text{cm}^{-1}$. The pseudogap anomaly is especially pronounced when the optical data are processed by what is known as the extended Drude formula [2, 29], where effective (i.e. depending on the frequency of the external field) scattering rate and current-carrier mass are introduced:

$$\frac{1}{\tau(\omega)} = \frac{\omega_{pl}^2}{4\pi}\ \text{Re}\left[\frac{1}{\sigma(\omega)}\right], \tag{1}$$

$$\frac{m^*(\omega)}{m} = -\frac{1}{\omega}\frac{\omega_{pl}^2}{4\pi}\ \text{Im}\left[\frac{1}{\sigma(\omega)}\right], \tag{2}$$

with $\sigma(\omega)$ the observed complex-valued conductivity, ω_{pl} the plasma frequency, and m the free-electron mass. Strictly

speaking, the use of equations (1) and (2) implies only data processing, since one uses them for representation in the form $1/\tau(\omega)$ and $m^*(\omega)$ instead of two other characteristics, the real and imaginary parts of the conductivity. Accordingly, $\tau(\omega)$ and $m^*(\omega)$ have no deep physical meaning. Nevertheless, such a representation of experimental data is extremely popular among researchers.

Figure 7b depicts the results of such processing of the data presented in Fig. 7a [30]. Clearly, at temperatures below $T^* \sim 450$ K the effective scattering rate decreases dramatically in the range of external-field frequencies below 700 cm^{-1}, while at higher frequencies $1/\tau(\omega)$ increases linearly with ω, demonstrating anomalous non-Fermi liquid behavior. It is the presence of this dip in $1/\tau(\omega)$ that reflects, as it is commonly assumed, the presence of a pseudogap in optical data. At the same time, taking into account the above notes, it should be noted that the data on $m^*(\omega)$ depicted in Fig. 7b do not allow for any graphic interpretation.

Similar behavior of $1/\tau(\omega)$ is also observed in the data on the transverse optical conductivity $\sigma_c(\omega)$ in almost all studied HTSC cuprates in the region of underdoped compositions [2, 29].

2.4 Fermi surface and ARPES

The most dramatic effects related to pseudogap formation manifest themselves in angle-resolved photoemission spectroscopy (ARPES) experiments [4, 5]. Such experiments play the leading role in studies of the topology of the Fermi surface of HTSC cuprates [4, 31, 32] and are practically the only source of information in this area of research.

Figure 8 depicts the data, gathered by Ino et al. [33], on the Fermi surface of the $La_{2-x}Sr_xCuO_4$ system for two different compositions. In the overdoped state ($x = 0.3$) the Fermi surface is electronic with its center at point $\Gamma(0,0)$ of the Brillouin zone. As x decreases, the topology of the surface changes, so that for the optimal concentration of Sr and in the underdoped state ($x = 0.1$) it becomes a hole surface with its center at point $Y(\pi,\pi)$. It is this latter topology of the Fermi surface that is observed in almost all ARPES experiments for the majority of other HTSC cuprates.

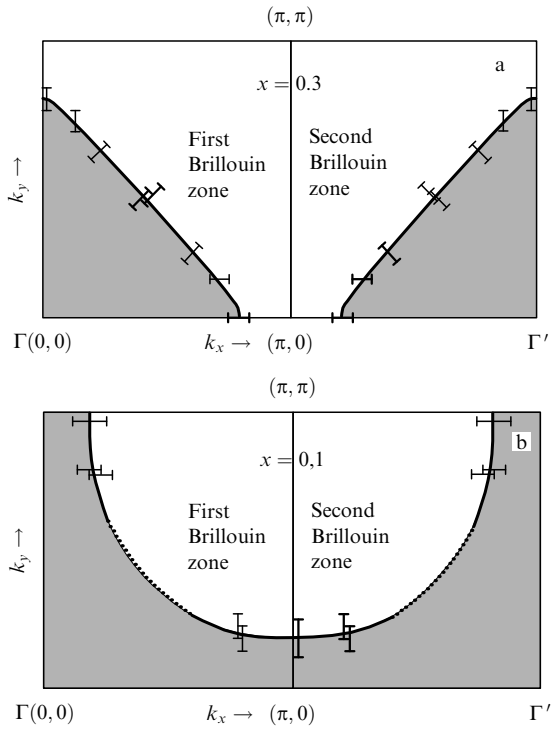

Figure 8. Fermi surfaces of $La_{2-x}Sr_xCuO_4$ for the overdoped (a) and underdoped (b) cases [33].

An interesting example is presented in Fig. 9, taken from the paper of Gatt et al. [34]. It depicts the hole Fermi surface of the Bi-2212 system in the overdoped state, a system that has been most thoroughly studied by the ARPES method. A distinctive feature here is the discovery in these experiments of large flat regions of the Fermi surface that are orthogonal to the symmetric directions YM. This result was corroborated independently by Feng et al. [35] for an optimally doped system. The presence of flat regions on the Fermi surface may be extremely important in developing microscopic theories of the electronic properties of HTSC systems.

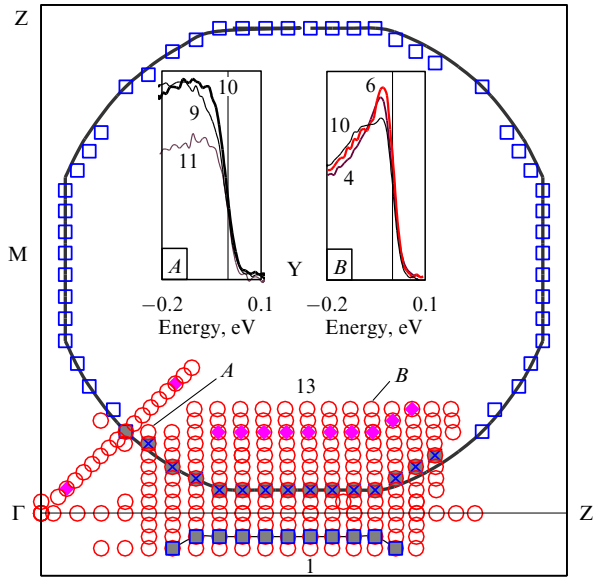

Figure 9. Fermi surface of overdoped Bi-2212 [34]. The small circles indicate the points at which the measurements were taken.

If we ignore these details, then, to a rather rough approximation, the topology of the Fermi surface and the spectrum of elementary excitations in the CuO_2 plane, which are observed in ARPES, can be described fairly well by the strong-coupling model:

$$\varepsilon_{\mathbf{k}} = -2t(\cos k_x a + \cos k_y a) - 4t' \cos k_x a \cos k_y a\,, \qquad (3)$$

where $t \approx 0.25$ eV is the transport integral between nearest neighbors; t' is the transport integral between next nearest neighbors, which can vary from $t' \approx -0.4t$ for $YBa_2Cu_3O_{7-\delta}$ to $t' \approx -0.25t$ for $La_{2-x}Sr_xCuO_4$; and a is the (square-) lattice constant.

Very recently the above simple picture was substantially revised by several researchers [35–38]. They used new ARPES data obtained with synchrotron radiation whose energy was higher than that used in previous experiments. The researchers claim that the Fermi surface of Bi-2212 is electronic with its center at point Γ. The main disagreement with the earlier data is related to the most interesting, from our viewpoint, neighborhood of the point $(0,\pi)$ in the reciprocal space. These results met with strong opposition

from other groups of ARPES experimenters [39–43]. The problem is being actively debated, but in the present review we will keep to the traditional interpretation.

Since there are several good reviews describing the observations of pseudogap anomalies in ARPES [3–5], we will only briefly describe the main qualitative statements. The ARPES intensity (the energy distribution of photoelectrons) is in fact defined as follows [4]:

$$I(\mathbf{k},\omega) = I_0(\mathbf{k}) f(\omega) A(\mathbf{k},\omega)\,, \tag{4}$$

where $\mathbf{k}$ is the momentum in the Brillouin zone, ω is the energy of the initial state measured from the Fermi level (the chemical potential)[7], and $I_0(\mathbf{k})$ incorporates kinematic factors and the square of the matrix element of the electron–photon interaction and, to a rough approximation, is kept constant. The quantity

$$A(\mathbf{k},\omega) = -\frac{1}{\pi}\,\mathrm{Im}\,G(\mathbf{k},\omega+\mathrm{i}\delta)\,, \tag{5}$$

with $G(\mathbf{k},\omega)$ the Green function, is the carrier spectral density. The Fermi distribution function $f(\omega) = [\exp(\omega/T)+1]^{-1}$ reflects the fact that electrons from occupied states participate in the photoemission process. Thus, to the rough approximation mentioned earlier, we can say that it is the product $f(\omega)A(\mathbf{k},\omega)$ that is directly measured in ARPES experiments; thus, we get direct information about the spectral properties of single-particle excitations of the system.

Figure 10 depicts typical ARPES data for the $Bi_2Sr_2CaCu_2O_8$ system [44] obtained for three different points on the Fermi surface at different temperatures. The presence of a gap (pseudogap) manifests itself in the shift (to the left) of the threshold (leading edge) of the energy distribution of photoelectrons from the sample, as compared to the reference spectrum of a good metal (Pt). Clearly, the gap closes at different temperatures for different values of $\mathbf{k}$, and the size (width) of the gap decreases with the departure from the $(0,0)-(0,\pi)$ direction. In the direction of the zone's diagonal $(0,0)-(\pi,\pi)$ there is no pseudogap. At low temperatures this agrees fairly well with the picture of d-pairing, well established in numerous experiments involving HTSC cuprates [45–47]. What is important, however, is that the 'gap' in ARPES data is also observed at temperatures much higher the superconducting transition temperature T_c.

Figure 11 depicts the angular behavior of the gap width in the Brillouin zone and the temperature dependence of the maximum size of the gap for a number of samples of Bi-2212 of different compositions, as obtained from ARPES data by Ding et al. [48]. Clearly, in the case of the general d-wave symmetry, the gap in the spectrum of an optimally doped system vanishes virtually at $T = T_c$, while in the spectrum of underdoped samples there appear 'tails' of the temperature dependence of the gap in the region $T > T_c$, which are quite similar to those shown in Fig. 3. Qualitatively we can say that the formation of a pseudogap anisotropic in the reciprocal space at $T > T_c$, which is continuously transformed into a superconducting gap at $T < T_c$, leads to the 'destruction' of the Fermi surface of underdoped samples even at $T < T^*$ in regions surrounding point $(0,\pi)$ (and symmetric with respect to this point), with the width of these regions increasing as the temperature decreases [49].

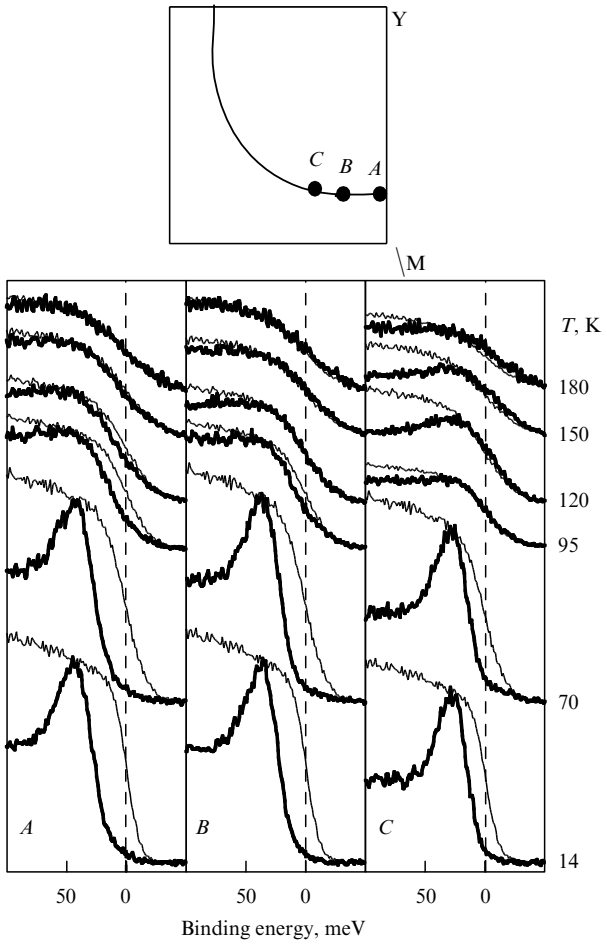

Figure 10. ARPES spectra at three different points A, B, and C on the Fermi surface of Bi-2212 for an underdoped sample with $T_c = 85$ K. The light lines represent the spectrum of a reference Pt sample (data of Norman et al. [44]).

Of course, the most interesting problem is here the evolution of the spectral density $A(\mathbf{k}_F,\omega)$ at the Fermi surface. Under fairly weak assumptions, this function can be extracted from ARPES data [49]. It there is electron–hole symmetry, we have $A(\mathbf{k}_F,\omega) = A(\mathbf{k}_F,-\omega)$ (which is always true near the Fermi surface and actually occurs when $|\omega|$ is smaller than several tenths of meV), so that combining $f(-\omega) = 1 - f(-\omega)$ and equation (4) with $\mathbf{k} = \mathbf{k}_F$ immediately yields $I(\omega) + I(-\omega) = A(\mathbf{k}_F,\omega)$. Hence the spectral density on the Fermi surface can be directly obtained from experiment by means of constructing a symmetrized spectrum $I(\omega) + I(-\omega)$. As an example, in Fig. 12 we depict the data of Norman et al. [50] for an underdoped sample of Bi-2212 with $T_c = 83$ K and an overdoped sample with $T_c = 82$ K at different temperatures. Clearly, a pseudogap manifests itself in the form of a characteristic 'double-humped' structure of the spectral density, which appears (for an undoped system) at temperatures much higher than T_c.

Note that well-defined quasiparticles correspond to a fairly narrow peak in the spectral density $A(\mathbf{k}_F,\omega)$ at $\omega = 0$. Such behavior is almost never encountered in HTSC cuprates, at least at temperatures higher than T_c. This fact, however, is not very surprising, since it is difficult to imagine well-defined quasiparticles in systems at $T > 100$ K, almost

[7] In a real experiment ω is measured with respect to the Fermi level of a good metal of the Pt or Ag type that is in electrical contact with the sample.

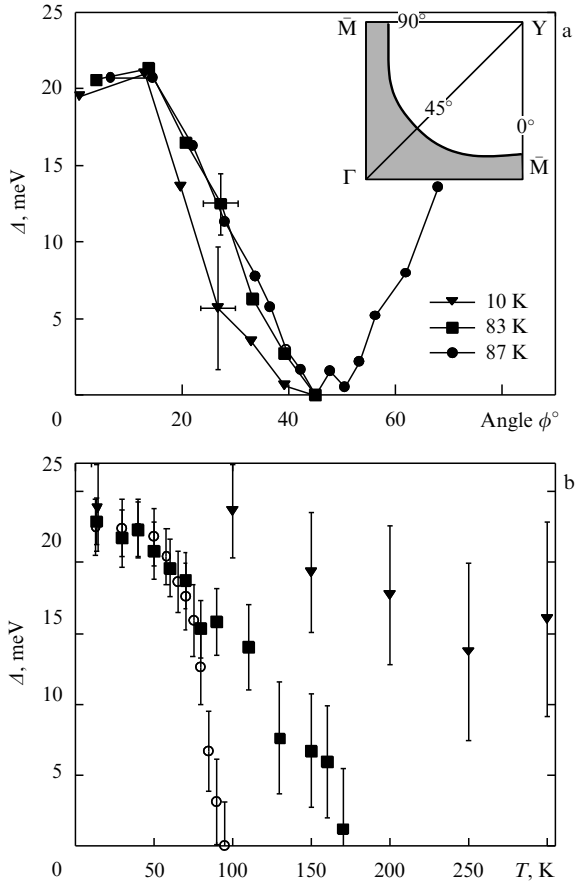

Figure 11. Angular and temperature dependences of the energy gap in Bi-2212 obtained from ARPES data [49] for samples with $T_c = 87$ K (almost optimally doped), $T_c = 83$ K, and $T_c = 10$ K (underdoped): (a) the size of the ARPES gap measured at different points of the Fermi surface (depicted in the inset) whose positions are determined by the polar angle ϕ measured from the direction $\Gamma\bar{M}$ (the d-symmetry of the gap is clearly visible); (b) the temperature dependence of the maximum gap measured near point $\bar{M}$.

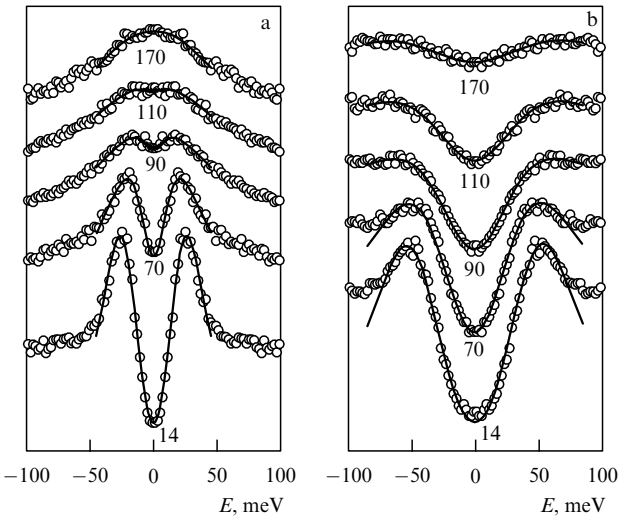

Figure 12. Symmetric ARPES spectra for (a) an overdoped sample of Bi-2212 with $T_c = 82$ K and (b) an underdoped sample with $T_c = 83$ K at the point of intersection of the Fermi surface and the zone boundary $(0, \pi) - (\pi, \pi)$ [50].

without exception. Nevertheless, the resolution of modern ARPES devices apparently provides reasons to state that the width of the corresponding peak is larger than the experimental resolution, so the problem is accessible to experiments [51]. It turns out that in the superconducting phase, at $T \ll T_c$, near the point of intersection of the Fermi surface and the diagonal of the Brillouin zone [the $(0, 0) - (\pi, \pi)$ direction] there appears a fairly sharp spectral-density peak corresponding to well-defined quasiparticles [51]. Near point $(0, \pi)$ the Fermi surface is 'destroyed' by a superconducting gap corresponding to d-type pairing, which results in a double-peaked structure of the spectral density.

The smooth evolution of an ARPES pseudogap at $T > T_c$ into a superconducting gap corresponding to d-pairing at $T < T_c$ is often considered an argument in favor of the superconducting nature of the pseudogap state. Most likely this is not the case, however. In this connection note the very interesting work of Ronning et al. [52], who carried out ARPES investigations of the dielectric oxide $Ca_2CuO_2Cl_2$, which is structurally similar to La_2CuO_4 and becomes a high-T_c superconductor when doped with sodium or potassium. ARPES measurements in this system also proved to be possible in the dielectric phase due to the good quality of the samples' surface. A remarkable feature of this paper [52] is that it apparently presents the first report of an observation of the 'residual' Fermi surface in this Mott insulator, which is, naturally, 'blocked' by a gap (probably of the Mott – Hubbard type). At the same time, Ronning et al. [52] observed a strong anisotropy of this gap in the reciprocal space with a d-type symmetry, closely resembling similar data on HTSC oxides in the metallic phase. It is quite natural to assume that this anisotropic gap is of the same nature as the pseudogap in the high-energy region, say, in Bi-2212 [52]. Clearly there is no Cooper pairing in the insulator.

2.5 Other experiments

The pseudogap behavior also manifests itself in other experiments, such as Raman scattering of light on electrons [53] or magnetic scattering of neutrons [54]. All these data point, in one way or another, to a substantial suppression of the density of states of single-particle excitations near the Fermi level of underdoped HTSC cuprates at temperatures below T^*, i.e. even in the normal phase. In view of the shortage of space, we will not discuss these data in greater detail, the more so that good reviews can be found in the above-cited papers and in Ref. [2].

3. Theoretical models of the pseudogap state

3.1 Scattering on short-range-order fluctuations: Qualitative ideas

As noted in the Introduction, there are two main theoretical scenarios for explaining the pseudogap anomalies in HTSC systems. The first one is based on the model of Cooper pair formation above the superconducting transition temperature (precursor pairing), while the second one assumes that the origin of the pseudogap state is related to short-range-order fluctuations of a 'dielectric' type (e.g. antiferromagnetic or of the charge-density-wave type), which exist in the underdoped-composition range and strongly scatter electrons, which leads to a pseudogap transformation of the electron spectrum. We believe the second scenario to be preferable, which follows

from both the experimental data[8] discussed in Section 2 and the simple fact that all pseudogap anomalies intensify as underdoping increases, i.e. as the system departs from the phase-diagram region optimal for superconductivity and approaches the region of the dielectric (antiferromagnetic) phase.

Let us examine a typical Fermi surface of carriers in the CuO_2 plane depicted in Fig. 13a. The phase transition to the antiferromagnetic state doubles the lattice spacing and leads to the emergence of a 'magnetic' Brillouin zone in the reciprocal space, depicted in Fig. 13a by dashed lines. If the carrier spectrum is given by equation (3) with $t' = 0$, then for a half-filled zone the Fermi surface is a square coinciding with the boundaries of the magnetic zone, so that there is complete nesting, i.e. translation by the antiferromagnetism vector $\mathbf{Q} = (\pm\pi/a, \pm\pi/a)$ results in the alignment of the flat regions of the Fermi surface. At $T = 0$ the electron spectrum is unstable: a gap opens everywhere on the Fermi surface and the system passes to a dielectric state caused by an antiferromagnetic spin-density wave (SDW)[9]. Such ideas form the basis for the popular explanation of antiferromagnetism in HTSC cuprates — see, for instance, Ref. [55]. A review of such models can be found in Ref. [56]. In the case of the Fermi surface depicted in Fig. 13a, as antiferromagnetic long-range order emerges, then, according to the general principles of band theory [57], at the points of intersection of constant-energy surfaces (the Fermi surface, for one thing) and the boundaries of the new (magnetic) Brillouin zone, these surfaces experience a discontinuity related to the opening of a gap in the spectrum at points connected by the vector $\mathbf{Q}$.

In the region of the phase diagram of HTSC cuprates of interest to us there is no antiferromagnetic long-range order, but there are convincing experimental indications that everywhere below the T^*-line there are well-developed fluctuations of antiferromagnetic short-range order. The model of a 'nearly antiferromagnetic' Fermi liquid [58, 59] introduces an effective interaction between electrons and spin fluctuations, which is described by the dynamic spin susceptibility $\chi_{\mathbf{q}}(\omega)$, whose shape is determined through matching to the data of NMR experiments [46, 60]:

$$V_{\text{eff}}(\mathbf{q}, \omega) = g^2 \chi_{\mathbf{q}}(\omega) \approx \frac{g^2 \xi^2}{1 + \xi^2 (\mathbf{q} - \mathbf{Q})^2 - \mathrm{i}\omega/\omega_{\text{sf}}}, \qquad (6)$$

where g is the coupling constant, ξ is the correlation length of the spin fluctuations, $\mathbf{Q} = (\pm\pi/a, \pm\pi/a)$ is the vector of antiferromagnetic ordering in the dielectric phase, and ω_{sf} is the characteristic spin–fluctuation frequency.

Since the dynamic spin susceptibility $\chi_{\mathbf{q}}(\omega)$ has peaks at wave vectors lying in the neighborhood of $(\pm\pi/a, \pm\pi/a)$, two types of quasiparticles appear in the system — 'hot' quasiparticles, whose momenta are in the neighborhood of 'hot' spots on the Fermi surface (Fig. 13a) and whose energies obey the inequality

$$|\varepsilon_{\mathbf{k}} - \varepsilon_{\mathbf{k}+\mathbf{Q}}| < \frac{v_{\text{F}}}{\xi} \qquad (7)$$

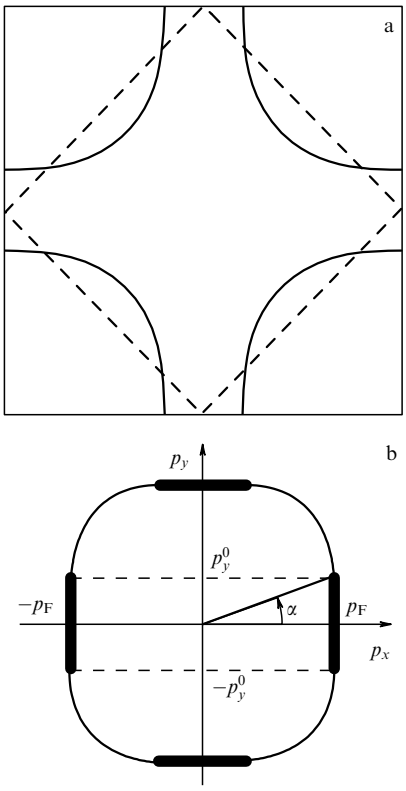

Figure 13. (a) Fermi surface in the Brillouin zone and the hot-point model. The dashed lines depict the boundaries of the magnetic Brillouin zone, which emerges as a result of lattice-spacing doubling related to the appearance of antiferromagnetism. The 'hot' spots are the points of intersection of the Fermi surface and the boundaries of the magnetic zone. (b) The Fermi surface in the hot-regions model (the hot spots, or hot regions, are depicted by heavy lines). The width of the hot spots is of order $\sim \xi^{-1}$. Angle α determines the size of a hot region [63], with $\alpha = \pi/4$ corresponding to a square Fermi surface.

(v_{F} is the velocity on the Fermi surface), and 'cold' quasiparticles, whose momenta are near the regions of the Fermi surface that surround the diagonals of the Brillouin zone, $|p_x| = |p_y|$, and do not satisfy the condition (7) [14]. This terminology reflects the fact that quasiparticles in the vicinity of 'hot' spots experience a strong scattering of order $\mathbf{Q}$ due to interactions with spin fluctuation [Eqn (6)], while for quasiparticles with momenta far from the 'hot' spots this interaction is fairly weak. In what follows we call such a model the 'hot'-spots model[10].

We will see that the correlation length ξ of antiferromagnetic short-range-order fluctuations, described by equation (6), plays an important role. Note that in real HTSC systems ξ is usually not very large and can vary from $2a$ to $8a$ [61, 62].

Depending on the type of the compound and doping level, the characteristic spin-fluctuation frequency ω_{sf} ranges from 10 to 100 K [61, 62], so that in the most part of the pseudogap region on the phase diagram the condition $\pi T \gg \omega_{\text{sf}}$ holds fairly well. This condition makes it possible to ignore the spin dynamics and restrict the analysis to the quasistatic approx-

[8] For instance, in my opinion, the tunneling experiments of Krasnov et al. [21, 22] bear out almost entirely the 'superconducting' scenario of pseudogap formation.

[9] A similar picture emerges in the case of dielectrization due to charge-density-wave formation.

[10] Note that the antiferromagnetic nature of the fluctuations is unimportant for further analysis, and the model is of a more general nature. What is important here is the strong scattering of electrons by vectors fairly close to the vector $\mathbf{Q}$, which 'moves' electrons from one side of the Fermi surface to the other. Both charge-density-wave (CDW) fluctuations and structural fluctuations may be responsible for such processes.

imation [11]:

$$V_{\text{eff}}(\mathbf{q}) = \widetilde{W}^2 \frac{\xi^2}{1+\xi^2(\mathbf{q}-\mathbf{Q})^2}\,, \tag{8}$$

where $\widetilde{W}$ is an effective parameter with dimensions of energy, which can be written in the model of antiferromagnetic fluctuations [14] as

$$\widetilde{W}^2 = g^2 T \sum_{m,\mathbf{q}} \chi_{\mathbf{q}}(\mathrm{i}\omega_m) = \frac{g^2\langle \mathbf{S}_i^2\rangle}{3}\,, \tag{9}$$

with $\mathbf{S}_i$ the spin at the lattice site (the Cu ion in the CuO_2 plane for HTSC cuprates).

In what follows both $\widetilde{W}$ and ξ are interpreted as phenomenological parameters of the theory. In particular, $\widetilde{W}$ defines the effective width of the pseudogap. Here we will not attempt to develop a complete microscopic theory of the pseudogap state. In what follows we will mainly model the corresponding transformation of the electron spectrum and its effect on the physical properties of the system (e.g. on superconductivity).

All calculations can be made much simpler if instead of (8) we use a model interaction of the form

$$V_{\text{eff}}(\mathbf{q}) = W^2 \frac{2\xi^{-1}}{\xi^{-2}+(q_x-Q_x)^2}\frac{2\xi^{-1}}{\xi^{-2}+(q_y-Q_y)^2}\,, \tag{10}$$

where $W^2 = \widetilde{W}^2/4$ (the first to use this approach were Kampf and Schrieffer [11]). Qualitatively, equation (10) closely resembles (8) and quantitatively differs very little in the most interesting region $|\mathbf{q}-\mathbf{Q}| < \xi^{-1}$. A similar (but somewhat different in form) effective interaction was used by Schmalian et al. [14]. Actually, such an approach effectively reduces the problem to a one-dimensional one.

The scattering on antiferromagnetic fluctuations in HTSC cuprates not always reaches its intensity maximum at the vector $\mathbf{Q} = (\pi/a, \pi/a)$ commensurate with the spacing of the original lattice; generally, the vector $\mathbf{Q}$ may correspond to incommensurate scattering. The observed topology of the Fermi surface with flat regions of the type depicted in Fig. 9 suggests another model of scattering on short-range-order fluctuations of the antiferromagnetic type [12], which we will call the hot-region model [63]. Let us assume that the Fermi surface of a two-dimensional electronic system has a shape as depicted in Fig. 13b. The size of the 'hot' regions is determined by the angular parameter α. It is well known that the presence of flat regions on the Fermi surface leads to the instability of the system against the formation of charge- or spin-density waves, with the onset of a corresponding long-range order and the formation of a (dielectric) energy gap in these regions. However, we are interested in situations characteristic of the fluctuation region of the corresponding phase diagram, when there is no long-range order [13]. Such a model of the Fermi surface has been applied to HTSC cuprates for a fairly long time by Virosztek and Ruvalds [65], Ruvalds et al. [66], and Zheleznyak et al. [67], who, in particular, analyze in detail the microscopic criteria for the existence of the antiferromagnetic and superconducting phases (the phase diagram).

We assume that short-range-order fluctuations are static and have a Gaussian form [14] and define the correlation function of these fluctuations as follows (in a manner similar to that assumed in Ref. [11]):

$$S(\mathbf{q}) = \frac{1}{\pi^2}\frac{\xi^{-1}}{(q_x-Q_x)^2+\xi^{-2}}\frac{\xi^{-1}}{(q_y-Q_y)^2+\xi^{-2}}\,. \tag{11}$$

Here ξ is again the correlation length of fluctuations, and the scattering vector is taken in the form $Q_x = \pm 2k_{\text{F}}$, $Q_y = 0$ or $Q_y = \pm 2k_{\text{F}}$, $Q_x = 0$. We also assume that only the electrons from the flat ('hot') regions of the Fermi surface, which are shown in Fig. 13b, interact with these fluctuations, and the scattering is actually one-dimensional. In particular, at $\alpha = \pi/4$ we simply have a square Fermi surface, and the problem becomes purely one-dimensional. When $\alpha < \pi/4$, the Fermi surface has 'cold' regions, where the scattering is either absent or very weak. The effective interaction of the electrons from the 'hot' regions with fluctuations will be described here by the quantity $(2\pi)^2 W^2 S(\mathbf{q})$, where the parameter W with dimensions of energy again determines the energy scale (width) of the pseudogap [15]. The choice of the scattering vector, $\mathbf{Q} = (\pm 2k_{\text{F}}, 0)$ or $\mathbf{Q} = (0, \pm 2k_{\text{F}})$, generally implies that there are incommensurate fluctuations, since the Fermi momentum $p_{\text{F}} = \hbar k_{\text{F}}$ is generally not related to the reciprocal lattice spacing. The commensurate case can also be considered with this model (see Ref. [63]).

As noted earlier, the main idea of the models under consideration consists in examining strong scattering on short-range-order fluctuations, which, in accordance with (6), (10), or (11), is effectively finite only within a limited region of the reciprocal space, of the size of order ξ^{-1}, surrounding 'hot' spots or regions, which leads to a pseudogap transformation of the electron spectrum in such regions [16].

Let us qualitatively examine the nature of the corresponding changes in the one-electron spectral density (5). In the standard Fermi-liquid theory [69], the one-electron Green function of a metal has the form

$$G(\omega, \mathbf{k}) = \frac{Z_{\mathbf{k}}}{\omega - \xi_{\mathbf{k}} - \mathrm{i}\gamma_{\mathbf{k}}} + G_{\text{incoh}}\,, \tag{12}$$

[11] According to the terminology used by Schmalian et al. [14], this corresponds to a 'weak' pseudogap.

[12] Since in what follows we ignore, for the sake of simplicity, the spin structure of the interaction, our reasoning is, strictly speaking, applicable to the case of interaction of electrons and short-range-order CDW-type fluctuations. This simplification, however, is unimportant from the viewpoint of the qualitative manifestations of the pseudogap transformation of the electron spectrum. Note that some researchers suggest using the interaction with CDW-type fluctuations to explain the anomalies of HTSC cuprates in the region of interest as an alternative to the spin fluctuation model [64].

[13] The assumption that there are flat regions on the Fermi surface is not really important in the model but substantially simplifies calculations, which can be done, at least in principle, for the more realistic 'hot'-spots model.

[14] Strictly speaking, this assumption is applicable only when the temperature is sufficiently high.

[15] We can say that we introduce an effective coupling constant of the electron-fluctuation interaction in the form $W_{\mathbf{p}} = W\big[\theta(p_x^0 - p_x)\times\theta(p_x^0 + p_x) + \theta(p_y^0 - p_y)\theta(p_y^0 + p_y)\big]$ (Fig. 13b).

[16] A similar situation is realized in molten metals and semiconductors, where the information about the lost crystalline structure is saved in the so-called structure factor and leads to a characteristic maximum in this factor in momentum space. This quantity plays a determinant role in the Ziman and Edwards theory of the electronic structure of liquid metals and semiconductors [68]. However, in 3D isotropic liquids averaging over angles usually leads to a significant weakening of pseudogap effects.

where $\xi_{\mathbf{k}} = \varepsilon_{\mathbf{k}} - \mu$ is the quasiparticle energy measured from the Fermi level (chemical potential) μ, and $\gamma_{\mathbf{k}}$ is the quasiparticle damping. For the residue at the pole, $0 < Z_{\mathbf{k}} < 1$, and G_{incoh} is the nonsingular (incoherent) contribution of many-particle excitations. Then the corresponding spectral density is given by the formula

$$A(\omega, \mathbf{k}) = \frac{1}{\pi} Z_{\mathbf{k}} \frac{\gamma_{\mathbf{k}}}{(\omega - \xi_{\mathbf{k}})^2 + \gamma_{\mathbf{k}}^2} + \ldots, \tag{13}$$

where the ellipsis stands for the more or less invariable contribution originating from G_{incoh}, and the quasiparticle spectrum manifests itself in a narrow (as $\gamma_{\mathbf{k}}$ is small) Lorentzian peak. The situation is illustrated in Fig. 14a.

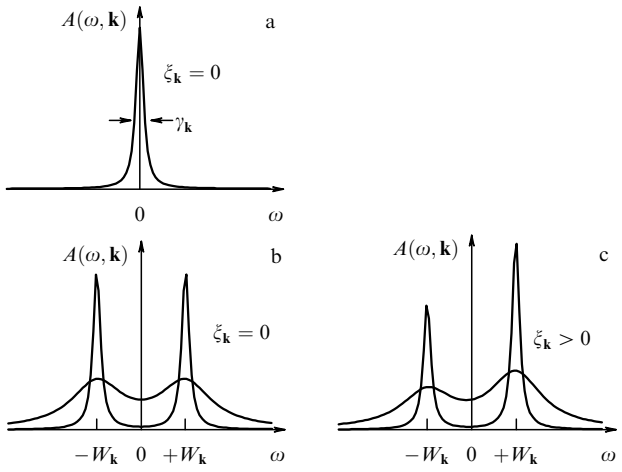

Figure 14. Qualitative picture of the evolution of the spectral density. (a) Normal metal (Fermi liquid) at $\xi_{\mathbf{k}} = 0$, i.e. at the Fermi surface. (b) Two narrow peaks corresponding to 'Bogolyubov' quasiparticles in a system with a dielectric gap $W_{\mathbf{k}}$ (in the presence of long-range CDW- or SDW-type order). The diffuse maxima represent a system without long-range order (pseudogap behavior), $\xi_{\mathbf{k}} = 0$ (at the Fermi surface). (c) The same as in (b) but with $\xi_{\mathbf{k}} > 0$, i.e. above the Fermi surface. In this case the spectral density acquires a characteristic asymmetry.

If long-range order (say, of SDW- or CDW-type) sets in in the system, a (dielectric) gap of width $W_{\mathbf{k}}$ opens in the spectrum of the elementary excitations of the system (the dependence on $\mathbf{k}$ emphasizes the possibility of the appearance of a finite gap only within a certain portion of the Fermi surface), and the one-electron Green function becomes the well-known Gor'kov function [55, 56] to which the decay $\Gamma_{\mathbf{k}}$ can be added:

$$G(\omega, \mathbf{k}) = \frac{u_{\mathbf{k}}^2}{\omega - E_{\mathbf{k}} + \mathrm{i}\Gamma_{\mathbf{k}}} + \frac{v_{\mathbf{k}}^2}{\omega + E_{\mathbf{k}} - \mathrm{i}\Gamma_{\mathbf{k}}}, \tag{14}$$

where the excitation spectrum is

$$E_{\mathbf{k}} = \sqrt{\xi_{\mathbf{k}}^2 + W_{\mathbf{k}}^2} \tag{15}$$

and where we have introduced the Bogolyubov coefficients

$$u_{\mathbf{k}}^2 = \frac{1}{2}\left(1 + \frac{\xi_{\mathbf{k}}}{E_{\mathbf{k}}}\right), \tag{16}$$

$$v_{\mathbf{k}}^2 = \frac{1}{2}\left(1 - \frac{\xi_{\mathbf{k}}}{E_{\mathbf{k}}}\right). \tag{17}$$

Then the spectral density is given by the formula

$$A(\omega, \mathbf{k}) = \frac{u_{\mathbf{k}}^2}{\pi} \frac{\Gamma_{\mathbf{k}}}{(\omega - E_{\mathbf{k}})^2 + \Gamma_{\mathbf{k}}^2} + \frac{v_{\mathbf{k}}^2}{\pi} \frac{\Gamma_{\mathbf{k}}}{(\omega + E_{\mathbf{k}})^2 + \Gamma_{\mathbf{k}}^2} + \ldots, \tag{18}$$

where we now have *two* peaks, narrow as $\Gamma_{\mathbf{k}}$ is small and corresponding to 'Bogolyubov' quasiparticles.

Now suppose that there is no CDW- or SDW-type long-range order but strong scattering on fluctuations with the corresponding wave vectors is present [cf. (6) and (10) or (11)]. Then it is easy to imagine that, in the region of momentum space where a dielectric gap opens in the presence of long-range order, the spectral density retains a 'recollection' (or 'premonition') of this gap in the form of a characteristic 'double-humped' structure, as shown qualitatively in Fig. 14 [17]. Here the width of the peaks is naturally determined by a parameter like v_{F}/ξ, i.e. by the reciprocal time of transit of an electron through a region of size ξ in which the 'dielectric' order is effectively retained. Thus, the qualitative picture of the process agrees fairly well with the ARPES data displayed in Fig. 12. Below we will see that a systematic treatment of the problem leads to precisely these results. Our further discussion will be devoted to justifying this qualitative scheme and to deriving various corollaries.

3.2 Recurrent procedure for the Green functions

The model of the pseudogap state considered here is actually a two-dimensional generalization of the pseudogap model proposed many years ago by Lee et al. [70] and the present author [71–73] for the fluctuation region of the Peierls (CDW) structural transition in one-dimensional systems [18]. In particular, in Refs [71, 72] an exact solution of the problem was derived in the limit of very large correlation lengths of short-range-order fluctuations, $\xi \to \infty$, while in Ref. [73] a generalization to the case of finite ξ was carried out. What sets Refs [71–73] apart from the paper by Lee et al. [70] is the allowance for all diagrams of the Feynman series in the theory of perturbation in the interaction with fluctuations. A two-dimensional generalization of this approach was carried out by Schmalian et al. [14] and Kuchinskiĭ and Sadovskiĭ [15] in the 'hot'-spots model, while in the hot-region model such a generalization is trivial because the problem can be completely reduced to a one-dimensional one.

The contribution of an arbitrary diagram for the self-energy part of a one-electron Green function of the Nth order in the interaction (10) or (11) with fluctuations can be approximately written as follows [15]:

$$\Sigma^{(N)}(\varepsilon_n, \mathbf{p}) = W^{2N} \prod_{j=1}^{2N-1} \frac{1}{\mathrm{i}\varepsilon_n - \xi_j + \mathrm{i}n_j v_j \varkappa}, \tag{19}$$

where in the hot-point model $\xi_j = \xi_{\mathbf{p}+\mathbf{Q}}$ and $v_j = |v_{\mathbf{p}+\mathbf{Q}}^x| + |v_{\mathbf{p}+\mathbf{Q}}^y|$ for j odd and $\xi_j = \xi_{\mathbf{p}}$ and $v_j = |v_{\mathbf{p}}^x| + |v_{\mathbf{p}}^y|$ for j even, while in the hot-region model, $\xi_j = (-1)^j \xi_{\mathbf{p}}$ and $v_j = v_{\text{F}}$. In equation (19) we have introduced the reciprocal correlation length $\varkappa = \xi^{-1}$, n_j is the number of interaction lines encompassing the jth Green function in the given

[17] In what follows, the term 'non-Fermi-liquid behavior' will be used only in this, fairly limited, sense.

[18] In Ref. [71] this model was used to explain the appearance of a pseudogap in liquid semiconductors.

diagram, $\varepsilon_n = (2n+1)\pi T$, and, for the sake of definiteness, $\varepsilon_n > 0$.

Actually, equation (19) is a fairly successful ansatz for calculating the contribution of a diagram of any order. In this case any diagram with the interaction lines crossed proves to be equal to a diagram of the same order but without interaction-line crossing. Hence we can actually consider only diagrams without interaction-line crossing and allow for the diagrams with line crossing by introducing additional combinatorial factors at the interaction vertices. Such an approach was first used (in another problem) by Elyutin [74] and was then employed in Ref. [73] for a one-dimensional model of the pseudogap state. Equation (19) is not exact [75] and can be justified in the two-dimensional case only for certain topologies of the Fermi surface, such that the projections of the electron velocities at 'hot' spots linked by the vector $\mathbf{Q}$ have the same sign and hence $v_{\mathbf{p}}^x v_{\mathbf{p}+\mathbf{Q}}^x > 0$ and $v_{\mathbf{p}}^y v_{\mathbf{p}+\mathbf{Q}}^y > 0$ [15]. This condition is obviously invalid in the one-dimensional case and for a topology of the Fermi surface typical of HTSC cuprates (see Fig. 13a). However, as shown in Ref. [15], in such cases the use of equation (19) also leads to a satisfactory description, reproducing the well-known exact results for the limits $\xi \to \infty$ and $\xi \to 0$ [19].

As a result we arrive at the following recurrent relation (represented in the form of a continued fraction [73]) for the one-electron Green function:

$$G^{-1}(\varepsilon_n, \xi_{\mathbf{p}}) = G_0^{-1}(\varepsilon_n, \xi_{\mathbf{p}}) - \Sigma_1(\varepsilon_n, \xi_{\mathbf{p}}) , \tag{20}$$

$$\Sigma_k(\varepsilon_n, \xi_{\mathbf{p}}) = W^2 \frac{v(k)}{\mathrm{i}\varepsilon_n - \xi_k + \mathrm{i}kv_k\varkappa - \Sigma_{k+1}(\varepsilon_n, \xi_{\mathbf{p}})} . \tag{21}$$

The combinatorial factor

$$v(k) = k \tag{22}$$

corresponds to the case of commensurate fluctuations with $\mathbf{Q} = (\pm\pi/a, \pm\pi/a)$ (considered here) [73]. It is really easy to examine also the case of incommensurate fluctuations, where $\mathbf{Q}$ is not related to the reciprocal lattice spacing. In this case the contribution of the diagrams in which the interaction lines encompass an odd number of vertices is much smaller than that of the diagrams in which the interaction lines encompass an even number of vertices. Hence only the latter type of diagram can be taken into account [71–73]. In this case the recurrent relation (21) is still valid, but the combinatorics of the diagrams changes and so do the factors $v(k)$ [73]:

$$v(k) = \begin{cases} \dfrac{k+1}{2} & \text{for odd } k , \\ \dfrac{k}{2} & \text{for even } k . \end{cases} \tag{23}$$

Schmalian et al. [14] allowed for the spin structure of the interaction in the model of an 'almost antiferromagnetic' Fermi liquid (the spin–fermion model). It proves that allowing for this structure leads to a more complex combinatorics of the diagrams in the commensurate case $\mathbf{Q} = (\pm\pi/a, \pm\pi/a)$. More precisely, scattering with spin conservation yields formally commensurate combinatorics, while scattering with a spin flip is described by diagrams for the incommensurate case (a 'charged' random field, in the terminology of Schmalian et al. [14]). As a result, the recurrent relation for the Green function is still of the form (21), but the combinatorial factor $v(k)$ becomes [14]

$$v(k) = \begin{cases} \dfrac{k+2}{3} & \text{for odd } k , \\ \dfrac{k}{3} & \text{for even } k . \end{cases} \tag{24}$$

3.3 Spectral density and the density of states

The recurrence relations (20) and (21) are very convenient for numerical calculations. Fairly detailed calculations of spectral densities, ARPES characteristics, and densities of states have been carried out for different variants of the 'hot'-spots model [14, 15]. As a typical example, Fig. 15a depicts the results of Ref. [15] for the spectral density of carriers in the incommensurate case. Clearly, the spectral density near a 'hot' spot has the expected non-Fermi-liquid shape, and the quasiparticle concept does not work here. Far from a 'hot' spot the spectral density has a sharp peak corresponding to well-defined quasiparticles (a Fermi liquid). In Fig. 15b (taken from Ref. [14]) we depict the product of the distribution function by the spectral density for different points on the 'renormalized' Fermi surface determined from the equation $\varepsilon_{\mathbf{k}} - \mathrm{Re}\,\Sigma(\omega = 0, \mathbf{k}) = 0$, where the 'bare' spectrum $\varepsilon_{\mathbf{k}}$ was taken in the form (3) with $t = -0.25$ eV, $t' = -0.35t$, hole concentration $n_{\mathrm{h}} = 0.16$, coupling constant in (6) $g = 0.8$ eV, and correlation length $\xi = 3a$ (the commensurate case and the spin–fermion model). There are clearly full qualitative agreement with the ARPES data discussed above and a qualitatively different behavior near the 'hot' spot and far from it. Finally, in Fig. 16 (taken from Ref. [14]) we depict the positions of the maximum of $A(\omega, \mathbf{k})$ calculated in the spin–fermion model with interaction (6) (the static limit) for two different hole concentrations, and the corresponding ARPES data of Marshall et al. [79] for the $Bi_2Sr_2Ca_{1-x}Dy_xCu_2O_{8+\delta}$ system. The point is that for an ideal system of a Fermi-liquid type the positions of the maximum of the spectral density in the $(\omega, \mathbf{k})$ plane found from ARPES data actually determine the dispersion law for the corresponding quasiparticles (Fig. 14a). For an overdoped system the values $n_{\mathrm{h}} = 0.22$ and $\xi = a$ were taken. The results demonstrate branches of the spectrum, defined fairly well, in both the direction of the diagonal of the Brillouin zone and the direction $(0,0)-(\pi,0)$. For an underdoped system the values $n_{\mathrm{h}} = 0.16$ and $\xi = 3a$ were assumed. Here in the direction of the diagonal one can clearly see the intersection of the spectrum with the Fermi level, while near 'hot' spots, in the neighborhood of $(\pi, 0)$, the diffuse maximum of the spectral density remains approximately 200 meV below the Fermi level (a pseudogap). On the whole, agreement between the theoretical model and the experimental data can be considered quite satisfactory.

Now let us turn to the one-electron density of states

$$N(E) = \sum_{\mathbf{p}} A(E, \mathbf{p}) = -\frac{1}{\pi} \sum_{\mathbf{p}} \mathrm{Im}\, G^{\mathrm{R}}(E, \mathbf{p}) , \tag{25}$$

[19] In the least favorable case of a one-dimensional model, ansatz (19) yields a very good quantitative approximation, e.g., for the density of states, which becomes evident from a direct comparison [76] of the results of Ref. [73] for an incommensurate case with the results of the exact numerical simulation of the problem in question done by Bartosh and Kopietz [77] and Millis and Monien [78]. In a commensurate case, (19) does not describe only a Dyson singularity in the density of states are the center of the pseudogap [77, 78], which is certainly absent in the 2D case.

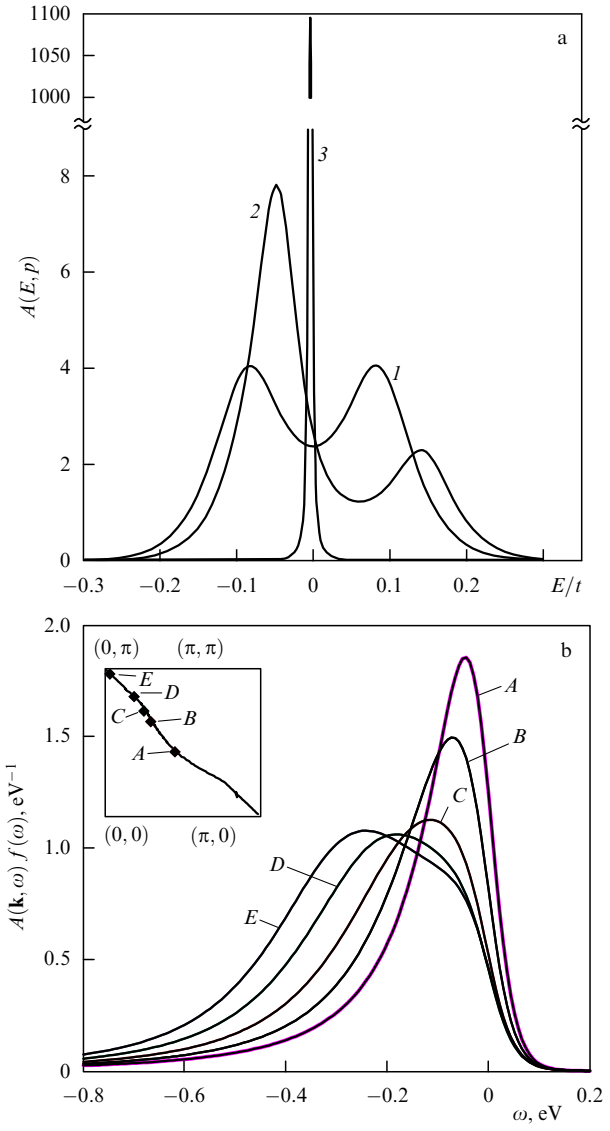

Figure 15. (a) Spectral density in the 'hot'-spots model, the case of incommensurate fluctuations, $\varkappa a = 0.01$ [15], at the 'hot' spot $p_x a/\pi = 0.142$, $p_y a/\pi = 0.587$ (curve *1*); near the 'hot' spot at $p_x a/\pi = 0.145$, $p_y a/\pi = 0.843$ (curve *2*); and far from the 'hot' spot at $p_x a/\pi = p_y a/\pi = 0.375$ (curve *3*). (b) The product of the spectral density by the Fermi distribution function at different points of the Fermi surface that are shown in the inset. The spin–fermion model, correlation length $\xi = 3a$ [14].

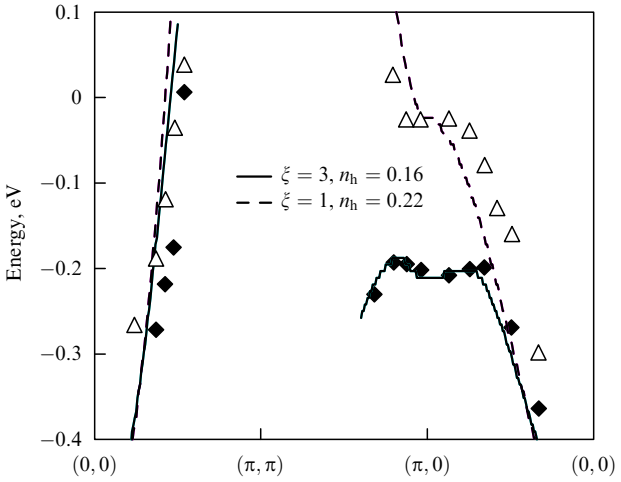

Figure 16. The position of the maximum in the spectral density as a function of the correlation length ξ and the hole concentration, calculated for the variant of the spin–fermion model under discussion [14], compared to the ARPES data of Ref. [79] for the $Bi_2Sr_2Ca_{1-x}Dy_xCu_2O_{8+\delta}$ system at $x = 1$ (triangles) and $x = 0.175$ (diamonds).

which is determined by an integral of $A(E, \mathbf{p})$ over the entire Brillouin zone. Detailed calculations of the density of states in the 'hot'-spots model were done in Ref. [15]. For a typical value $t'/t = -0.4$, a small dip (pseudogap) is observed in the density of states. The dip in the density of states only weakly depends on the correlation length ξ. At the same time, say at $t'/t = -0.6$ (which is not typical of HTSC cuprates), the Fermi surface does contain 'hot' spots, but a pseudogap in the density of states can hardly be identified. What is noticeable is the blurring of the Van Hove singularity, which exists in the absence of scattering on fluctuations.

In the hot-region model, the use of (20) and (21) leads to a spectral density quite similar in the 'hot' regions to that depicted in Fig. 15a [81, 82]. In the 'cold' regions of the Fermi surface the spectral density reduces to a Dirac delta function, which is typical of Fermi liquids (cf. Fig. 14a). The density of states is given by the formula

$$N(E) = -\frac{1}{\pi} N_0(0) \int_0^{2\pi} \frac{\mathrm{d}\phi}{2\pi} \int_{-\infty}^{\infty} \mathrm{d}\xi_{\mathbf{p}} \operatorname{Im} G^{\mathrm{R}}(E, \xi_{\mathbf{p}})$$
$$= \frac{4\alpha}{\pi} N_{\mathrm{W}}(E) + \left(1 - \frac{4\alpha}{\pi}\right) N_0(0)\,, \qquad (26)$$

where $N_0(0)$ is the density of states of free electrons on the Fermi level, and $N_{\mathrm{W}}(E)$ is the density of states in the one-dimensional problem (a square Fermi surface), found earlier in Refs [71–73].

Let us present more detailed results for a rather artificial limit of very long fluctuation correlation lengths, $\xi \to \infty$. This limit allows easily summing the entire perturbation series for an electron scattered on such fluctuations [71, 72] and obtaining the exact analytical solution for the one-electron Green function in the form [63]

$$G(\varepsilon_n, p) = \int_0^{\infty} \mathrm{d}D\, \mathcal{P}(D)\, \frac{\mathrm{i}\varepsilon_n + \xi_p}{(\mathrm{i}\varepsilon_n)^2 - \xi_p^2 - D(\phi)^2}\,, \qquad (27)$$

where $D(\phi)$ is defined for $0 \leqslant \phi \leqslant \pi/2$ as

$$D(\phi) = \begin{cases} D\,, & 0 \leqslant \phi \leqslant \alpha\,, \quad \dfrac{\pi}{2} - \alpha \leqslant \phi \leqslant \dfrac{\pi}{2}\,, \\ 0\,, & \alpha \leqslant \phi \leqslant \dfrac{\pi}{2} - \alpha\,. \end{cases} \qquad (28)$$

For other values of ϕ the quantity $D(\phi)$ is obviously defined from symmetry considerations in a manner similar to (28).

The amplitude of the dielectric gap D is a random quantity distributed according to the Rayleigh law [73] [its phase is also random and is distributed uniformly over the interval $(0, 2\pi)$]:

$$\mathcal{P}(D) = \frac{2D}{W^2} \exp\left(-\frac{D^2}{W^2}\right). \qquad (29)$$

Thus, in the 'hot' regions, the Green function has the shape of a 'normal' Gor'kov function averaged over fluctuations of the

dielectric gap D [distributed according to (29)], which are spatially uniform. Here the 'anomalous' Gor'kov function is zero due to the randomness of the phases of the dielectric gap D, which corresponds to the absence of long-range order in the system [20].

For finite correlation lengths ξ the amplitude of our one-dimensional 'periodic' random field is approximately constant over a length of order ξ, and its values in different regions of size $\sim\xi$ are random. An electron is effectively scattered only when it passes from one such region to another, which takes a characteristic time $\sim\xi/v_{\mathrm{F}}$ and leads to decay $\sim v_{\mathrm{F}}/\xi$. Interesting data on simulation of a random field in which the motion of the electron is treated within the framework of the one-dimensional variant of the model at hand can be found in Ref. [75].

Outside the 'hot' regions [the second inequality in (28)] the Green function (27) is simply the Green function of free electrons.

The density of states corresponding to (27) has the form (26), where

$$\frac{N_{\mathrm{W}}(E)}{N_0(0)} = \left|\frac{E}{W}\right| \int_0^{E^2/W^2} \mathrm{d}\zeta\, \frac{\exp(-\zeta)}{\sqrt{E^2/W^2-\zeta}} = 2\left|\frac{E}{W}\right| \exp\left(-\frac{E^2}{W^2}\right) \mathrm{Erfi}\left(\frac{E}{W}\right). \tag{30}$$

Here $\mathrm{Erfi}(x)$ is the error function of imaginary argument.

Figure 17 depicts diagrams of the density of states in our model for different values of the parameter α, i.e. for 'hot' regions of different sizes. Clearly, the pseudogap in the density of states becomes 'blurred' rather rapidly with the decrease in the size of 'hot' regions and is in general not very distinct. In a certain sense the effect of decreasing α is similar to the effect of decreasing correlation length ξ of the fluctuations [73], so that the above approximation $\xi\to\infty$ is, possibly, not a very strong limitation on the applicability of the model. The finiteness of ξ can easily be taken into account using (20) and (21), which additionally suppresses of the pseudogap as ξ decreases. Note the general qualitative agreement between the shape of the pseudogap in the density of states in the hot-region model and the shape of the pseudogap observed in tunnel experiments, which becomes evident if we look at Fig. 4.

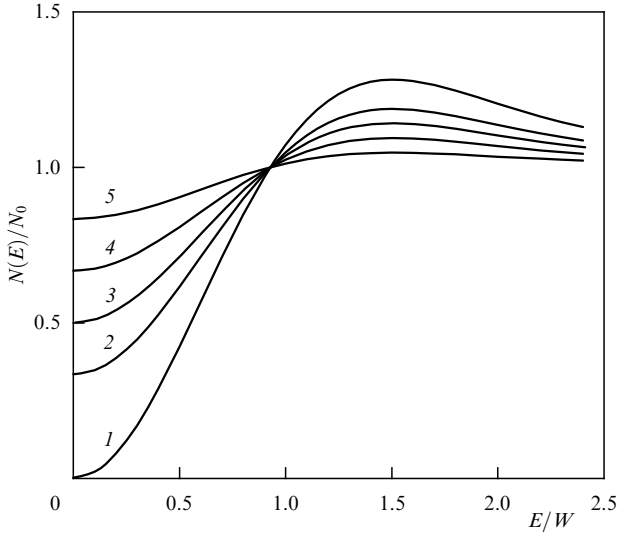

Figure 17. Density of electronic states for 'hot' regions of different sizes [63]: (*1*) $\alpha=\pi/4$, (*2*) $\alpha=\pi/6$, (*3*) $\alpha=\pi/8$, (*4*) $\alpha=\pi/12$, and (*5*) $\alpha=\pi/24$.

[20] Note that the pair averages of the anomalous functions are finite and contribute to the corresponding exact solution for the two-particle Green function [71, 72].

3.4 Two-particle Green function and optical conductivity

A remarkable feature of the models in question is the possibility of doing a fairly consistent calculation of the two-particle Green function of the electron in the field of random short-range-order fluctuations [80, 81] (see also Ref. [14]) that allows for *all* diagrams in the Feynman perturbation series. Since calculations in the hot-point model are fraught with serious difficulties related to the use of a 'realistic' current-carrier spectrum (3), we limit ourselves to a simplified analysis of the hot-region model [83].

We assume that in 'cold' regions of the Fermi surface there is weak static scattering of an arbitrary nature, whose rate we will describe by a phenomenological parameter γ assuming that always $\gamma\ll W$, so that in 'hot' regions this scattering can be ignored. Accordingly, in 'cold' regions the electron spectrum is described by the ordinary expressions for the Green functions in a system with weak scattering.

We begin with the limit $\xi\to\infty$, where the one-electron Green function has the form (27) and the two-particle Green function can also be found exactly by the methods described in Refs [71, 72].

The conductivity in the given model always consists of additive contributions from 'hot' and 'cold' regions, similar to (26). In particular, for the real part of the conductivity we have, as $\xi\to\infty$,

$$\mathrm{Re}\,\sigma(\omega) = \frac{4\alpha}{\pi}\,\mathrm{Re}\,\sigma_{\mathrm{W}}(\omega) + \left(1-\frac{4\alpha}{\pi}\right)\mathrm{Re}\,\sigma_{\mathrm{D}}(\omega), \tag{31}$$

where, with allowance for the results obtained in Refs [71, 72],

$$\mathrm{Re}\,\sigma_{\mathrm{W}}(\omega) = \frac{\omega_{\mathrm{pl}}^2}{4}\,\frac{W}{\omega^2}\int_0^{\omega^2/4W^2} \mathrm{d}\zeta\exp(-\zeta)\,\frac{\zeta}{\sqrt{\omega^2/4W^2-\zeta}}. \tag{32}$$

Here ω_{pl} is the plasma frequency, and

$$\mathrm{Re}\,\sigma_{\mathrm{D}}(\omega) = \frac{\omega_{\mathrm{pl}}^2}{4\pi}\,\frac{\gamma}{\omega^2+\gamma^2} \tag{33}$$

is the common Drude part of the conductivity due to 'cold' regions.

Even in this very simple approximation the ω-dependence of $\mathrm{Re}\,\sigma$ closely resembles the experimental data given in Refs [29, 30, 84, 85] and is characterized by a narrow Drude peak at low frequencies and a smooth maximum in the absorption through the pseudogap at $\omega\sim 2W$. As the rate γ of scattering on 'cold' regions increases, the characteristic Drude peak at low frequencies is more and more suppressed.

A more realistic case of a finite correlation length ξ of fluctuations of short-range 'antiferromagnetic' order in (11) can be analyzed using (20) and (21). The vertex part $J^{\mathrm{RA}}(\epsilon,\xi_{\mathbf{p}};\epsilon+\omega,\xi_{\mathbf{p}+\mathbf{q}})$, which determines the density–density response function (the two-particle Green function) in 'hot' regions, can be found by the following recurrent procedure (for more details see Refs. [80, 81] and also

Ref. [14]), which allows for all diagrams in the interaction with fluctuations:

$$J^{\mathrm{RA}}_{k-1}(\epsilon,\xi_{\mathbf{p}};\epsilon+\omega,\xi_{\mathbf{p}+\mathbf{q}}) = e + W^2 v(k) G^{\mathrm{A}}_k(\epsilon,\xi_{\mathbf{p}}) \times G^{\mathrm{R}}_k(\epsilon+\omega,\xi_{\mathbf{p}+\mathbf{q}}) J^{\mathrm{RA}}_k(\epsilon,\xi_{\mathbf{p}};\epsilon+\omega,\xi_{\mathbf{p}+\mathbf{q}}) \times \left(1 + 2\mathrm{i}v_{\mathrm{F}}\varkappa k\left\{\omega - (-1)^k v_{\mathrm{F}} q + v(k+1)W^2 \times \left[G^{\mathrm{A}}_{k+1}(\epsilon,\xi_{\mathbf{p}}) - G^{\mathrm{R}}_{k+1}(\epsilon+\omega,\xi_{\mathbf{p}+\mathbf{q}})\right]\right\}^{-1}\right). \quad (34)$$

Here e is the electron charge, the superscript R(A) indicates the retarded (advanced) Green function, and the vertex of interest to us is determined by zero order, $k = 0$, in the given recurrent procedure. The contribution to the conductivity from 'hot' regions, $\mathrm{Re}\,\sigma_{\mathrm{W}}(\omega)$, in (31) can now be calculated as in Refs [80, 81], while $\mathrm{Re}\,\sigma_{\mathrm{D}}(\omega)$ is still given by (33).

The typical results of calculations are depicted in Fig. 18 for the case of incommensurate fluctuations. The allowance for the combinatorics of the spin–fermion model leads to only slight quantitative changes. The general qualitative picture for the commensurate case is the same [83]. Conductivity is always characterized by the presence of a fairly narrow Drude peak at low frequencies, $\omega < \gamma$, which emerges from the 'cold' regions on the Fermi surface, and a gently sloping maximum at frequencies $\omega \sim 2W$, which corresponds to absorption through the pseudogap that opens in the 'hot regions. The Drude peak rapidly becomes blurred as γ increases. The dependence on the fluctuation correlation length $\xi = \varkappa^{-1}$ in the most interesting region of parameters is fairly weak. This qualitative picture closely resembles the pattern of experimental data for a broad range of HTSC systems [29, 30, 84, 85], with a typical example of such data depicted in Fig. 7. In the model in question we can calculate not only the real but also the imaginary part of the conductivity and, accordingly, the parameters of the extended Drude model (1) and (2) [86]. The calculated behavior of $1/\tau(\omega)$ is shown in the inset in Fig. 18 and represents the pseudogap behavior at frequencies $\omega < W$, similar to that depicted in Fig. 7b [21]. Thus, the resulting dip in $1/\tau(\omega)$ in the frequency range $\omega < W$ is a direct reflection of the presence of a pseudogap in the electron spectrum. It is probably easy to fit our results to the experimental data using the well-known values $\omega_{\mathrm{pl}} \sim 1.5-2.5$ eV and $2W \sim 0.1$ eV, as well as the values of γ determined experimentally from the width of the Drude peak, and varying the adjustable parameters α (the size of 'hot' regions) and ξ (for the latter quantity we can use the well-known estimates from other experiments [14]).

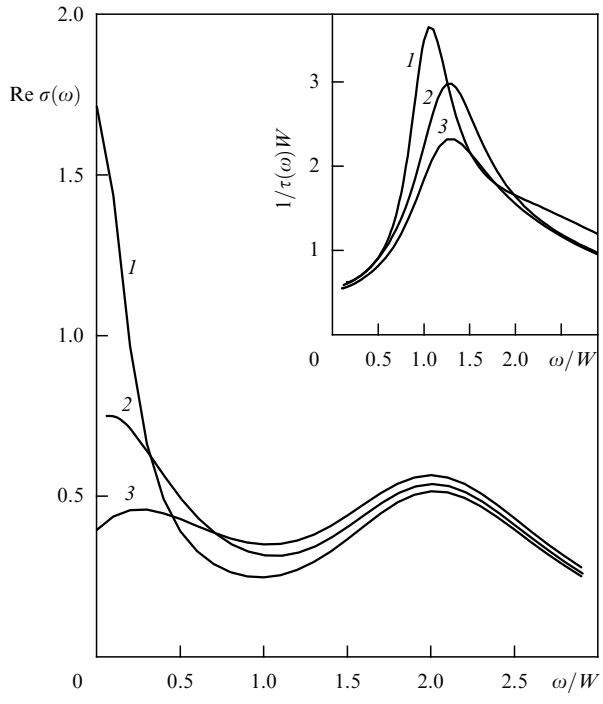

Figure 18. Real part of the conductivity as a function of the frequency of the external field at a fixed value of the correlation length $v_{\mathrm{F}}\varkappa = 0.5W$ for different values of γ (conductivity is in units of $\omega_{\mathrm{pl}}^2/4\pi W$): (*1*) $\gamma/W = 0.2$, (*2*) $\gamma/W = 0.5$, and (*3*) $\gamma/W = 1.0$. The size of the 'hot' regions is $\alpha = \pi/6$ [83]. The inset presents the calculated generalized scattering rate $1/\tau$ (in units of W) as a function of the frequency of the external field at a fixed $\gamma = 0.2W$ for different values of the correlation length: (*1*) $v_{\mathrm{F}}\varkappa = 0.1$, (*2*) $v_{\mathrm{F}}\varkappa = 0.5$, and (*3*) $v_{\mathrm{F}}\varkappa = 1.0$ [86].

4. Superconductivity in the pseudogap state

4.1 Gor'kov equations

At present there is no unified viewpoint on the mechanism of Cooper pairing in HTSC cuprates. What has been firmly established is only the fact of anisotropic pairing and d-wave symmetry of Cooper pairs [45–47], although even in this problem there are alternative viewpoints. Apparently, there is a tendency among most researchers to adhering to one or another variant of pairing caused by the exchange of spin (antiferromagnetic) fluctuations. A recent review of the attempts made in this direction can be found in Ref. [46]. A typical example of theories of this type is the model of a 'nearly antiferromagnetic' Fermi liquid (the spin–fermion model), which is being actively developed by Pines and his collaborators (see Refs [58, 59]). The model is based on the assumption that electrons interact with spin fluctuations, and the form of this interaction [Eqn (6)] is determined, as noted above, by means of fitting to NMR data [60]. This approach is being actively developed (the results of recent work in this area of research can be found in Refs [87–89]), and there are conclusive experimental facts in favor of this HTSC mechanism [46, 90]. At the same time, we have seen that the interaction (6) can also be responsible for the formation of a 'dielectric' pseudogap at sufficiently high temperatures. Unfortunately, so far there has been no studies that would consistently examine in conjunction the phenomenon of Cooper pairing and the formation of a pseudogap with the spin–fermion model.

On the other hand, rephrasing Landau's statement (quoted in Ref. [91]) that 'nobody has abrogated the Coulomb law for metals,' we can say that nobody has abrogated the electron–phonon interaction as well, and this interaction can serve as a possible microscopic pairing mechanism in HTSC. Reviews of the corresponding calculations with really impressive results can be found in Refs [91, 92] and in an earlier review by Ginzburg and Maksimov [93]. Perhaps the main difficulty of the pairing models based on the

[21] When $\omega > W$, the linear increase of $1/\tau(\omega)$ with frequency is not reproduced, but, to allow for such an increase, one can use a phenomenological substitution like $\gamma(\omega) = \gamma_0 + a\omega$, in the spirit of the theory of marginal Fermi liquids. The meaning of such a substitution is to 'allow' for inelastic scattering processes, completely ignored in our model.

electron – phonon interaction in HTSC cuprates is the d-wave symmetry of Cooper pairs (mentioned earlier). At the same time, interesting attempts have been made to explain anisotropic pairing based on the electron – phonon interaction [91, 92], and there are serious doubts on the efficiency of the spin-fluctuation mechanism [91].

I am not inclined to take sides in this discussion and believe that these (or similar [94]) fairly traditional mechanisms probably play a leading role in the microscopic theory of high-T_c superconductivity. In any case, in this review there will be no discussion of other, more radical, approaches like the Luttinger-liquid model [95], which has been developed for many years in different variants. The reason is that there are no well-established results and conclusions in these new approaches.

The above-discussed substantial transformation of the electron spectrum (pseudogap) has inevitably a strong effect on the properties of the system in the superconducting state. In the approach considered above, which is based on the scenario of pseudogap formation due to 'dielectric' (AFM, SDW, or CDW) type, short-range-order fluctuations, the discussion is about the effect of the pseudogap on superconductivity. In such an approach the investigation can be carried out without knowing the specifics of the pairing mechanisms, as is done, for instance, in analyzing the effects of such factors as structural disordering and the presence of impurities on superconductivity. From the physical viewpoint, the least justified in our further investigation is the above assumption that short-range-order fluctuations are static, since the dynamics of these fluctuations [say, within the model (6)] can play a leading role at low temperatures (in the superconducting phase), being possibly responsible for the very mechanism of Cooper pairing. We deliberately introduce appropriate simplifications, since for the time being it is impossible to get the full solution of the problem in a dynamical model. Moreover, our analysis will entirely be based on the simplified hot-region model[22] discussed in Section 3.1. For the sake of completeness, we consider s- and d-pairing in conjunction.

In view of what we have said, without concretizing the microscopic mechanism, we adopt the simple BCS-type model for the pairing interaction and assume that Cooper pairing occurs because of an attractive 'potential' of the following simple type:

$$V_{sc}(\mathbf{p},\mathbf{p}') = V(\phi,\phi') = -Ve(\phi)e(\phi')\,, \tag{35}$$

where ϕ is the polar angle determining the direction of the electron momentum $\mathbf{p}$ in the plane, and $e(\phi)$ is specified by the simple model dependence

$$e(\phi) = \begin{cases} 1 & \text{(s-pairing)}\,, \\ \sqrt{2}\cos 2\phi & \text{(d-pairing)}\,. \end{cases} \tag{36}$$

As usual, the attraction constant V is assumed to be nonzero within a certain layer of width $2\omega_c$ near the Fermi level (ω_c is the characteristic frequency of the quanta ensuring the attraction of electrons). The model interaction of type (35) has been successfully used by Borkowski and Hirschfeld [96] and Fehrenbacher and Norman [97] to analyze the effect of impurities on anisotropic Cooper pairing.

[22] This simplification is not very important. A similar analysis can be done within the hot-point model, but the complexity of the calculations increases substantially.

In this case the superconducting gap has the form

$$\Delta(\mathbf{p}) \equiv \Delta(\phi) = \Delta e(\phi)\,. \tag{37}$$

To avoid dealing with cumbersome formulas, we will hereinafter assume that Δ stands precisely for $\Delta(\phi)$ and will indicate the angular dependence explicitly only where this is required.

In the superconducting state, a theory that uses the interaction with AFM fluctuations (11) as a perturbation must be based on the 'free' normal and anomalous Green functions of the superconductor,

$$G_{00}(\varepsilon_n,\mathbf{p}) = -\frac{\mathrm{i}\varepsilon_n + \xi_{\mathbf{p}}}{\varepsilon_n^2 + \xi_{\mathbf{p}}^2 + |\Delta|^2}\,,$$
$$F_{00}^{+}(\varepsilon_n,\mathbf{p}) = \frac{\Delta^*}{\varepsilon_n^2 + \xi_{\mathbf{p}}^2 + |\Delta|^2}\,. \tag{38}$$

In this case, we can formulate a direct analog of the approximation (19) in the superconducting state [98]. The contribution of an arbitrary diagram of the Nth order in the interaction (10) to the normal or anomalous Green function has the form of the product of $N+1$ 'free' normal (G_{0k_j}) and anomalous ($F_{0k_j}^{+}$) Green functions, with frequencies and gaps renormalized in a certain way. Here k_j is the number of interaction lines encompassing the given jth (as counted from the beginning of the diagram) electron line. As in the normal phase, the contribution of any diagram is determined by a set of integers k_j, and each diagram with intersecting interaction lines is equal to a diagram of the same order without intersections of these lines. Hence we can again focus solely on diagrams without intersections, taking into account the contribution of other diagrams by introducing the same combinatorial factors $v(k)$ assigned to the interaction lines as in the normal phase. As a result, we arrive at an analog of the Gor'kov equations [69]. Accordingly, there emerge two coupled recurrent equations for the normal and anomalous Green functions:

$$G_k = G_{0k} + G_{0k}\widetilde{G}G_k - G_{0k}\widetilde{F}F_k^{+} - F_{0k}\widetilde{G}^{*}F_k^{+} - F_{0k}\widetilde{F}^{+}G_k\,,$$
$$F_k^{+} = F_{0k}^{+} + F_{0k}^{+}\widetilde{G}G_k - F_{0k}^{+}\widetilde{F}F_k^{+} + G_{0k}^{*}\widetilde{G}^{*}F_k^{+} + G_{0k}^{*}\widetilde{F}^{+}G_k\,, \tag{39}$$

where

$$\widetilde{G} = W^2 v\,(k+1)G_{k+1}\,, \qquad \widetilde{F}^{+} = W^2 v\,(k+1)F_{k+1}^{+}\,, \tag{40}$$

$$G_{0k}(\varepsilon_n,\mathbf{p}) = -\frac{\mathrm{i}\varepsilon_n + (-1)^k\xi_{\mathbf{p}}}{\tilde{\varepsilon}_n^2 + \xi_{\mathbf{p}}^2 + |\tilde{\Delta}|^2}\,, \quad F_{0k}^{+}(\varepsilon_n,\mathbf{p}) = \frac{\tilde{\Delta}^*}{\tilde{\varepsilon}_n^2 + \xi_{\mathbf{p}}^2 + |\tilde{\Delta}|^2} \tag{41}$$

and we have introduced the above-mentioned renormalized frequency $\tilde{\varepsilon}$ and gap $\tilde{\Delta}$,

$$\tilde{\varepsilon}_n = \eta_k\varepsilon_n\,, \qquad \tilde{\Delta} = \eta_k\Delta\,, \qquad \eta_k = 1 + \frac{kv_F\varkappa}{\sqrt{\varepsilon_n^2 + |\Delta|^2}}\,, \tag{42}$$

similar to those that appear when one considers superconductors with impurities [69].

The normal and anomalous Green functions of the superconductor, in which we are interested, are determined by (39) with $k = 0$ and represent the completely summed series of perturbation theory in the interaction of an electron

in the superconductor with antiferromagnetic short-range-order fluctuations.

Actually we are examining the Gor'kov-type Green functions averaged over the ensemble of random (Gaussian) short-range-order fluctuations in a similar way as is done in the problem of the effects of impurities on superconductivity [69]. Here we assume that the superconductor order parameter (the energy gap) Δ is self-averaging over these fluctuations, which makes it possible to average it irrespective of the electronic Green functions in the diagrammatic series. The usual arguments in favor of the possibility of such independent averaging is as follows [99–101]: the value of Δ varies over characteristic lengths of order $\xi_0 \sim v_F/\Delta$ (the coherence length of the BCS theory), while the Green functions vary rapidly over much smaller lengths, of the order of interatomic distances. Naturally, the last assumption does not hold if a new characteristic length $\xi \to \infty$ appears in the electronic subsystem. At the same time, in conditions where the AFM correlation length ξ is much smaller than ξ_0 (i.e. when AFM fluctuations correlate over distances shorter than the characteristic size of Cooper pairs), the assumption that Δ is self-averaging is valid, breaking down only in the region $\xi > \xi_0$. As a result, we can use the standard approach of the theory of disordered superconductors (the mean-field approximation, in the terminology of Ref. [102]). A possible manifestation of the non-self-averaging nature of Δ [102] will be considered below. Note that in real HTSC cuprates ξ is probably always of order ξ_0, so that they both are in the region that presents most difficulties for the theory.

4.2 Transition temperature and the temperature dependence of the gap

The energy gap of a superconductor is specified by the equation

$$\Delta(\mathbf{p}) = -T\sum_{\mathbf{p}'}\sum_{\varepsilon_n} V_{sc}(\mathbf{p},\mathbf{p}')\,F(\varepsilon_n,\mathbf{p}')\,. \qquad (43)$$

On flat sections of the Fermi surface the anomalous Green function can be found by applying the recurrent procedure (39). In the remaining ('cold') part of the Fermi surface there is no scattering on AFM fluctuations in our model, and the anomalous Green function has the form (38). The results of calculations of the temperature dependences of the energy gap for different values of the correlation length ξ of short-range order fluctuations can be found in Ref. [98]. These dependences are of a fairly traditional shape.

An equation for the superconducting transition temperature T_c immediately follows for (43) if $\Delta \to 0$. The dependences of T_c on the gap width W and the correlation length (the parameter $\varkappa = \xi^{-1}$) that were calculated in Ref. [98] are depicted in Fig. 19, where T_{c0} is the transition temperature in the absence of a pseudogap. In these calculations the value of α was rather arbitrarily taken equal to $\pi/6$, which is close to the experimental data of Gatt et al. [34].

The general qualitative conclusion is that a pseudogap suppresses superconductivity due to partial 'dielectrization' of the electron spectrum in the 'hot' regions of the Fermi surface. The suppression effect is maximum at $\varkappa = 0$ (infinite correlation length of AFM fluctuations [63, 102]) and decreases with the decrease of the correlation length, which completely agrees with the experimental phase diagram of HTSC systems. As noted above, the parameters of this model

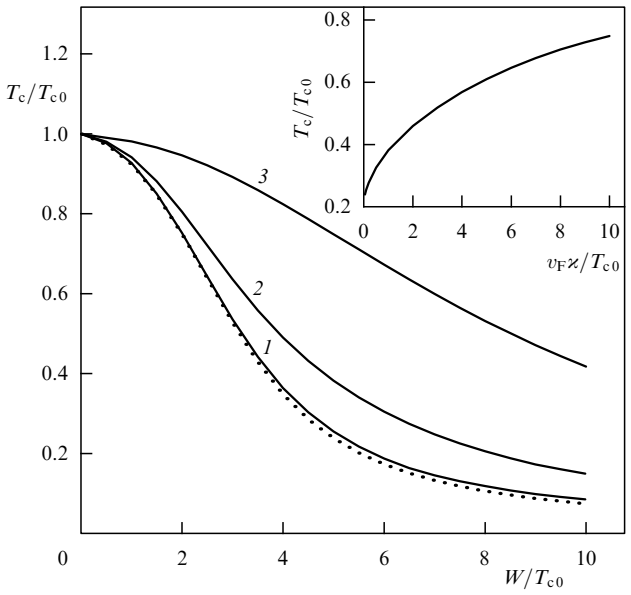

Figure 19. Dependence of the superconducting transition temperature on the pseudogap width W and the correlation length of antiferromagnetic fluctuations (the parameter $\varkappa = \xi^{-1}$): (*1*) $v_F\varkappa/W = 0.1$, (*2*) $v_F\varkappa/W = 1.0$, and (*3*) $v_F\varkappa/W = 10.0$. The dotted line corresponds to $\varkappa = 0$ [63]. The inset presents T_c as a function of $\varkappa$ at $W/T_{c0} = 5$ [98].

are phenomenological. For instance, the effective width of the pseudogap, $2W$, can probably be identified with the parameter E_g; experimental data on the magnitude of this parameter are depicted in Fig. 6 as a function of the doping level for the YBCO system. The data on the correlation length ξ and its temperature and concentration dependences are very incomplete. Indirectly the necessary information was extracted from data of NMR experiments [14, 60]. Direct data of neutron-scattering experiments are rather ambiguous. Nevertheless, as an example, we take the result of Balatsky and Bourges [103], who summarized the data on the width of the peak in neutron scattering by the vector $(\pi/a, \pi/a)$ in the YBCO system with varying oxygen content. It is only natural to identify the reciprocal of the peak width with ξ. These researchers found an interesting correlation between the superconducting transition temperature and the quantity ξ^{-1} defined in this manner (see Fig. 20). Obviously, this dependence is in direct correspondence to the dependence of T_c on $\varkappa = \xi^{-1}$ depicted in the inset in Fig. 19. A quantitative fitting of these data to the above-calculated dependences (which follow from the simple model of the pseudogap state considered here) is of course possible, but it requires taking into account rather ambiguous information about the concentration dependence of the parameter W. In particular, it is not quite clear whether there is any physical meaning in the vanishing of the quantity $E_g \sim W$ at a certain 'critical' carrier concentration, as shown in Fig. 6. The effect of the pseudogap can also disappear as a result of a proper decrease in the correlation length ξ, which leads to the 'filling' rather than 'collapse' of the pseudogap in the density of states. However, if we adopt the data [6] in Fig. 6 on the pseudogap width, then our parameter $2W$ changes from a value of order 700 K at a hole concentration of $p = 0.05$ to a value of order $T_c \sim 100$ K near the optimal concentration $p = 0.17$, vanishing at $p = 0.19$. If we use the microscopic expression (9) for the parameter W, which follows from the theory of a 'nearly

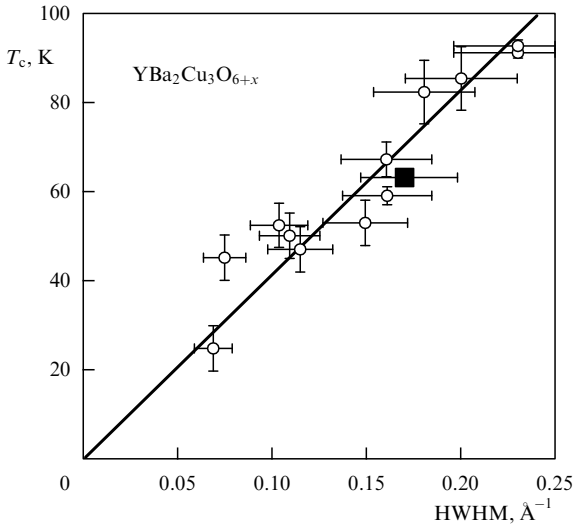

Figure 20. Superconducting transition temperature T_c as a function of the width of the peak in neutron scattering at $\mathbf{q} = (\pi/a, \pi/a)$, this width being identified with the reciprocal correlation length of short-range-order fluctuations [103].

antiferromagnetic' Fermi liquid, we can relate such a behavior of the concentration to the corresponding dependence for the local spin $\langle \mathbf{S}_i^2 \rangle$ on an ion of Cu. I am not aware any direct data of this kind, but it is worth mentioning a paper by Tallon [104], who demonstrated the vanishing of the effective interaction with antiferromagnetic spin fluctuations at $p = 0.19$ by means of processing the experimental data on NMR relaxation times.

We stress once more that the above theoretical results hold under the assumption that the superconducting order parameter (gap) is self-averaging over AFM fluctuations (the mean-field approximation, in the terminology of Ref. [102]), which is true if the correlation length is not too large, $\xi < \xi_0$, where ξ_0 is the coherence length of the superconductor (the size of the Cooper pairs at $T = 0$). We will see that, for $\xi \gg \xi_0$, non-self-averaging sets in, which results in the appearance of characteristic 'tails' in the temperature dependence of the averaged gap in the temperature range $T_c < T < T_{c0}$ [102].

4.3 Cooper instability

As is known, there is another way of finding the transition temperature, namely, from the equation for the Cooper instability of the normal phase,

$$1 - V\chi(0,0) = 0\,, \tag{44}$$

where $\chi(0,0)$ is the generalized Cooper susceptibility

$$\chi(\mathbf{q},0;T) = -T\sum_{\varepsilon_n}\sum_{\mathbf{p}} G(\varepsilon_n, \mathbf{p}+\mathbf{q})G(-\varepsilon_n,\mathbf{p}) \times e^2(\phi)\Gamma(\varepsilon_n,-\varepsilon_n,\mathbf{q})\,. \tag{45}$$

The problem is to calculate the 'triangular' vertex part $\Gamma(\varepsilon_n, -\varepsilon_n, \mathbf{q})$, which takes into account the interaction with AFM fluctuations. For a one-dimensional analog of our problem (and for real frequencies, $T = 0$), the corresponding recurrent procedure was formulated in Ref. [80]. For the two-dimensional model considered here, the optical conductivity was calculated on the basis of this procedure using the method discussed above [83]. The given procedure can be generalized fairly easily to the case of Matsubara frequencies [98]. For the sake of definiteness we will assume that $\varepsilon_n > 0$. Then we arrive at an expression similar to (34):

$$\Gamma_{k-1}(\varepsilon_n,-\varepsilon_n,\mathbf{q}) = 1 + W^2 v(k) G_k \bar{G}_k \times \left[1 + \frac{2\mathrm{i}kv_F\varkappa}{2\mathrm{i}\varepsilon_n - (-1)^k v_F q - W^2 v(k+1)(G_{k+1} - \bar{G}_{k+1})}\right] \times \Gamma_k(\varepsilon_n,-\varepsilon_n,\mathbf{q})\,,$$
$$\Gamma(\varepsilon_n,-\varepsilon_n,\mathbf{q}) \equiv \Gamma_0(\varepsilon_n,-\varepsilon_n,\mathbf{q})\,, \tag{46}$$

where $G_k = G_k(\varepsilon_n, \mathbf{p}+\mathbf{q})$ and $\bar{G}_k = G_k(-\varepsilon_n, \mathbf{p})$ can be calculated using (21).

In calculating T_c we are interested in the vertex at $\mathbf{q} = 0$. Then $\bar{G}_k = G_k^*$, and the vertices Γ_k become real-valued, which substantially simplifies the procedure (46).

We have the following exact relation of the type of the Ward identity [98]:

$$G(\varepsilon_n,\mathbf{p})G(-\varepsilon_n,\mathbf{p})\Gamma(\varepsilon_n,-\varepsilon_n,0) = -\frac{\operatorname{Im} G(\varepsilon_n,\mathbf{p})}{\varepsilon_n}\,. \tag{47}$$

Numerical calculations completely corroborate this relation and demonstrate perfect consistency between the recurrent procedures for the single-particle Green function and the vertex part. Formula (47) leads to a situation in which the equation for T_c obtained from the condition for the Cooper instability is equivalent to the equation obtained through linearizing the equation for the gap, although seemingly different recurrent procedures of taking into account AFM fluctuations were used in deriving these equations.

4.4 Ginzburg – Landau equations and the basic properties of superconductors with a pseudogap near T_c

The Ginzburg – Landau expansion for the difference in the free-energy densities between the superconducting and normal states can be written in the following standard form:

$$F_s - F_n = A|\Delta_\mathbf{q}|^2 + q^2 C|\Delta_\mathbf{q}|^2 + \frac{B}{2}|\Delta_\mathbf{q}|^4\,, \tag{48}$$

where $\Delta_\mathbf{q}$ is the amplitude of the Fourier transform of the order parameter,

$$\Delta(\phi,\mathbf{q}) = \Delta_\mathbf{q} e(\phi)\,. \tag{49}$$

The expansion (48) is determined by the diagrams of the loop expansion for the free energy in the field of order-parameter fluctuations with a small wave vector $\mathbf{q}$ [63].

We write the Ginzburg – Landau coefficients in the form

$$A = A_0 K_A\,; \qquad C = C_0 K_C\,; \qquad B = B_0 K_B\,, \tag{50}$$

where A_0, B_0, and C_0 denote the standard expressions for these coefficients in the case of isotropic s-pairing:

$$A_0 = N_0(0)\,\frac{T - T_c}{T_c}\,, \qquad C_0 = N_0(0)\,\frac{7\zeta(3)}{32\pi^2}\,\frac{v_F^2}{T_c^2}\,,$$
$$B_0 = N_0(0)\,\frac{7\zeta(3)}{8\pi^2 T_c^2}\,. \tag{51}$$

All features of this model related to pseudogap formation are contained in the dimensionless coefficients K_A, K_C, and K_B. In

the absence of a pseudogap all these coefficients are equal to unity, and only in the case of d-pairing we have $K_B = 3/2$.

Now we go back to the generalized Cooper susceptibility (45). Using it allows us to easily write the coefficients K_A and K_C in the form [98]

$$K_A = \frac{\chi(0,0;T) - \chi(0,0;T_c)}{A_0}\,, \tag{52}$$

$$K_C = \lim_{q\to 0} \frac{\chi(\mathbf{q},0;T_c) - \chi(0,0;T_c)}{q^2 C_0}\,. \tag{53}$$

Then all calculations can be done via the recurrent procedure (46).

Generally, the situation with the coefficient B is complicated. Significant simplifications are possible if we limit ourselves to the case $q = 0$ in the order $|\Delta_{\mathbf{q}}|^4$, as is usually done. Then the coefficient B can be found directly from the anomalous Green function F, for which we already have the recurrent procedure (39) [98].

In the limit $\xi \to \infty$, all Ginzburg–Landau coefficients can be obtained in an analytic form [63] using the exact solution (discussed above) for the Green function of the pseudogap state.

The Ginzburg–Landau equations determine two characteristic lengths of a superconductor: the coherence length and the depth of magnetic-field penetration. The coherence length for a given temperature, $\xi(T)$, gives the characteristic scale of inhomogeneities in the order parameter Δ:

$$\xi^2(T) = -\frac{C}{A}\,. \tag{54}$$

In the absence of a pseudogap,

$$\xi^2_{\mathrm{BCS}}(T) = -\frac{C_0}{A_0}\,, \tag{55}$$

$$\xi_{\mathrm{BCS}}(T) \approx 0{,}74\,\frac{\xi_0}{\sqrt{1 - T/T_c}}\,, \tag{56}$$

where $\xi_0 = 0.18 v_{\mathrm{F}}/T_c$. For the model we consider here,

$$\frac{\xi^2(T)}{\xi^2_{\mathrm{BCS}}(T)} = \frac{K_C}{K_A}\,. \tag{57}$$

The corresponding dependences of $\xi^2(T)/\xi^2_{\mathrm{BCS}}(T)$ on the pseudogap width W and the fluctuation correlation length (the parameter $\varkappa$) for the case of d-pairing are given in Ref. [98]; they are fairly smooth, and the variations in the ratio (57) are relatively small.

For the depth of magnetic-field penetration for a superconductor without a pseudogap we have

$$\lambda_{\mathrm{BCS}}(T) = \frac{1}{\sqrt{2}}\,\frac{\lambda_0}{\sqrt{1 - T/T_c}}\,, \tag{58}$$

where $\lambda_0^2 = mc^2/(4\pi n e^2)$ is the penetration depth at $T = 0$. Generally,

$$\lambda^2(T) = -\frac{c^2}{32\pi e^2}\,\frac{B}{AC}\,. \tag{59}$$

Then we have from our model:

$$\frac{\lambda(T)}{\lambda_{\mathrm{BCS}}(T)} = \left(\frac{K_B}{K_A K_C}\right)^{1/2}. \tag{60}$$

The dependences of this quantity on the pseudogap width and the correlation length for the case of d-pairing can also be found in Refs. [98], and the corresponding variations of (60) are also fairly small.

Near T_c the upper critical field H_{c2} is determined in terms of the Ginzburg–Landau coefficients as follows:

$$H_{c2} = \frac{\phi_0}{2\pi\xi^2(T)} = -\frac{\phi_0}{2\pi}\,\frac{A}{C}\,, \tag{61}$$

where $\phi_0 = c\pi/e$ is the fluxoid. Then the slope of the curve of the upper critical field near T_c is

$$\left|\frac{\mathrm{d}H_{c2}}{\mathrm{d}T}\right|_{T_c} = \frac{24\pi\phi_0}{7\zeta(3)v_{\mathrm{F}}^2}\,T_c\,\frac{K_A}{K_C}\,. \tag{62}$$

The diagrams representing the dependence of the upper-critical-field slope $|\mathrm{d}H_{c2}/\mathrm{d}T|_{T_c}$ at the temperature T_{c0} on the effective width W of the pseudogap and the correlation-length parameter $\varkappa$ are given in Ref. [98]. At sufficiently large correlation lengths, the field slope rapidly decreases with the pseudogap width. However, at fairly short correlation lengths, this parameter may slowly increase at small pseudogap widths. At a fixed pseudogap width, the slope of H_{c2} increases appreciably as the fluctuation correlation length decreases.

Finally, let us examine the specific-heat discontinuity at the transition point:

$$\frac{C_s - C_n}{\Omega} = \frac{T_c}{B}\left(\frac{A}{T - T_c}\right)^2, \tag{63}$$

where C_s and C_n are, respectively, the specific heats of the superconducting and normal states, and Ω is the sample's volume. At T_{c0} (in the absence of a pseudogap, or $W = 0$) we have

$$\left(\frac{C_s - C_n}{\Omega}\right)_{T_{c0}} = N(0)\,\frac{8\pi^2 T_{c0}}{7\zeta(3)}\,. \tag{64}$$

Then the relative specific-heat discontinuity in this model can be written as

$$\frac{(C_s - C_n)_{T_c}}{(C_s - C_n)_{T_{c0}}} = \frac{T_c}{T_{c0}}\,\frac{K_A^2}{K_B}\,. \tag{65}$$

The corresponding dependences on the effective pseudogap width W and the correlation-length parameter $\varkappa$ for the case of d-pairing are depicted in Fig. 21. Clearly, the specific-heat discontinuity rapidly decreases with increasing pseudogap width and, on the other hand, increases as the correlation length of AFM fluctuations decreases.

For superconductors with s-pairing the dependences of the physical quantities considered here are similar, and the only difference is in a larger scale of W over which the changes take place, which corresponds to a greater stability of isotropic superconductors against partial 'dielectrization' of the electron spectrum caused by pseudogap formation in the 'hot' regions of the Fermi surface [63, 102].

These results are in full qualitative agreement with the data on the specific-heat discontinuity [6, 18, 19] discussed above. As seen from Fig. 2, the discontinuity rapidly decreases with the transition to the region of underdoped compositions, where the pseudogap grows according to the data depicted in Fig. 6.

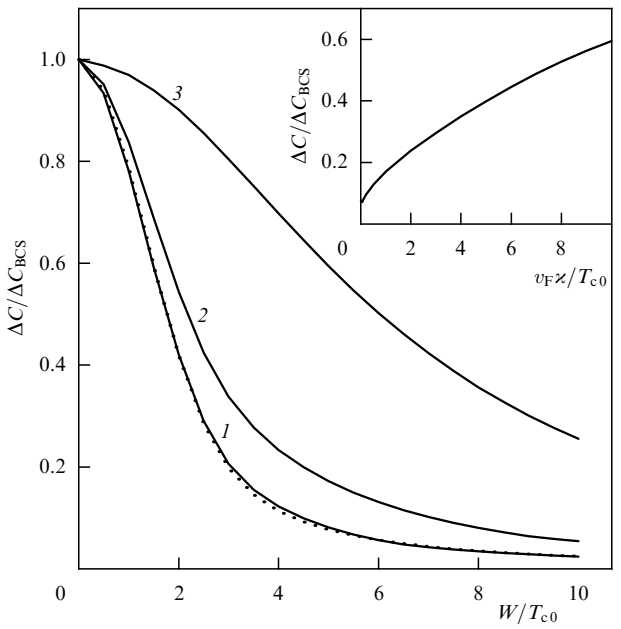

Figure 21. Specific-heat discontinuity as a function of the gap width W and the correlation length of AFM fluctuations (the parameter $\varkappa = \xi^{-1}$): (*1*) $v_F\varkappa/W = 0.1$, (*2*) $v_F\varkappa/W = 1.0$, and (*3*) $v_F\varkappa/W = 10.0$. The dotted curve corresponds to $\varkappa = 0$ [63]. The inset presents the specific-heat discontinuity as a function of $\varkappa$ at $W/T_{c0} = 5$.

4.5 Effects of the non-self-averaging nature of the order parameter

Our study of superconductivity was based on the assumption that the superconducting order parameter Δ is a self-averaging quantity. This assumption is justified only if the correlation length ξ of short-range-order (AFM) fluctuations is short compared to the characteristic size of the Cooper pairs, ξ_0 (the coherence length of the BCS theory). The opposite limit, $\xi \gg \xi_0$, can be treated within the scope of the exactly solvable model of the pseudogap state with $\xi \to \infty$, which has been described above in the variant of the hot-region model in equations (27) and (29) [102].

We begin with the problem of superconductivity in a system that has a *fixed* dielectric gap D in the 'hot' regions of the Fermi surface. The problem of superconductivity in a system with partial dielectrization of the spectrum in selected regions of the Fermi surface has been studied by many researchers (e.g. see Refs [105, 106]), and in a model closest to our case, by Bilbro and McMillan [107], whose results we can use here. We will employ the simplest model of pairing — equations (35) and (36) of the BCS theory.

If the value of the dielectric gap D in the 'hot' regions of the Fermi surface is fixed, the equation of our model for the superconducting gap Δ in the case of s-pairing assumes the form

$$1 = \lambda \int_0^{\omega_c} d\xi \left\{ \tilde{\alpha}\, \frac{\tanh\left[\sqrt{\xi^2 + D^2 + \Delta^2(D)}/2T\right]}{\sqrt{\xi^2 + D^2 + \Delta^2(D)}} + (1-\tilde{\alpha})\, \frac{\tanh\left[\sqrt{\xi^2 + \Delta^2(D)}/2T\right]}{\sqrt{\xi^2 + \Delta^2(D)}} \right\}, \quad (66)$$

where $\lambda = VN_0(0)$ is the dimensionless coupling constant of the pairing interaction, and $\tilde{\alpha} = 4\alpha/\pi$. The first term on the right-hand side of equation (66) corresponds to the contribution of 'hot' (dielectric) regions in which the electron spectrum has the form [107] $E_p = (\xi_p^2 + D^2 + \Delta^2)^{1/2}$, while the second term represents the contribution of 'cold' (metallic) regions, where the spectrum is the same as in the BCS theory: $E_p = (\xi_p^2 + \Delta^2)^{1/2}$. Equation (66) yields the superconducting gap $\Delta(D)$ at a fixed value of the dielectric gap D, which is finite in 'hot' regions.

In the case of d-pairing a similar equation has the form

$$1 = \lambda \frac{4}{\pi} \int_0^{\omega_c} d\xi \times \left\{ \int_0^{\alpha} d\phi\, e^2(\phi)\, \frac{\tanh\left[\sqrt{\xi^2 + D^2 + \Delta^2(D)e^2(\phi)}/2T\right]}{\sqrt{\xi^2 + D^2 + \Delta^2(D)e^2(\phi)}} + \int_{\alpha}^{\pi/4} d\phi\, e^2(\phi)\, \frac{\tanh\left[\sqrt{\xi^2 + \Delta^2(D)e^2(\phi)}/2T\right]}{\sqrt{\xi^2 + \Delta^2(D)e^2(\phi)}} \right\}. \quad (67)$$

These equations show that $\Delta(D)$ decreases with increasing D, and $\Delta(0)$ coincides with the ordinary gap Δ_0 in the absence of dielectrization in flat regions, i.e., the gap that appears at a temperature $T = T_{c0}$ specified by the equation

$$1 = \lambda \int_0^{\omega_c} d\xi\, \frac{\tanh(\xi/2T_{c0})}{\xi}, \quad (68)$$

for both s- and for d-pairing.

As $D \to \infty$, the first terms on the right-hand sides of equations (66) and (67) vanish, so that the corresponding equations for $\Delta_\infty = \Delta(D \to \infty)$ are

$$1 = \lambda \int_0^{\omega_c} d\xi\, (1-\tilde{\alpha})\, \frac{\tanh\left(\sqrt{\xi^2 + \Delta_\infty^2}/2T\right)}{\sqrt{\xi^2 + \Delta_\infty^2}} \quad \text{(s-pairing)}, \quad (69)$$

$$1 = \lambda \frac{4}{\pi} \int_0^{\omega_c} d\xi \int_{\alpha}^{\pi/4} d\phi \times e^2(\phi)\, \frac{\tanh\left[\sqrt{\xi^2 + \Delta_\infty^2 e^2(\phi)}/2T\right]}{\sqrt{\xi^2 + \Delta_\infty^2 e^2(\phi)}} \quad \text{(d-pairing)}. \quad (70)$$

Equation (69) coincides with the equation for a gap at $D = 0$ with the 'renormalized' coupling constant $\tilde{\lambda} = \lambda(1-\tilde{\alpha})$, so that for the case of s-pairing we have

$$\Delta_\infty = \Delta_0\left[\tilde{\lambda} = \lambda(1-\tilde{\alpha})\right], \quad (71)$$

and, accordingly, a nonzero gap with $D \to \infty$ emerges for $T < T_{c\infty}$:

$$T_{c\infty} = T_{c0}\left[\tilde{\lambda} = \lambda(1-\tilde{\alpha})\right]. \quad (72)$$

In the case of d-pairing, equation (70) yields

$$T_{c\infty} = T_{c0}\left[\tilde{\lambda} = \lambda(1-\alpha_d)\right], \quad (73)$$

where

$$\alpha_{\mathrm{d}} = \tilde{\alpha} + \frac{\sin \pi\tilde{\alpha}}{\pi} \tag{74}$$

is the 'effective' fraction of flat regions in the case of d-pairing. Thus, if $T < T_{\mathrm{c}\infty}$, the gap does not vanish for all values of D and decreases from Δ_0 to Δ_∞ as D increases. For $T_{\mathrm{c}\infty} < T < T_{\mathrm{c}0}$, the gap differs from zero only for $D < D_{\max}$. The corresponding dependences of Δ on D can easily be found by numerically solving equations (66) and (67).

In our model of the pseudogap state, the dielectric gap D is a random rather than fixed quantity distributed according to (29). The above equations must be averaged over these fluctuations. Here we can directly calculate the superconducting gap averaged over the fluctuations of D:

$$\langle\Delta\rangle = \int_0^\infty \mathrm{d}D\, \mathcal{P}(D)\Delta(D) = \frac{2}{W^2}\int_0^\infty \mathrm{d}D\, D \exp\left(-\frac{D^2}{W^2}\right)\Delta(D)\,. \tag{75}$$

In this case, the above-described behavior of $\Delta(D)$ leads to a situation in which the averaged gap (75) differs from zero until $T = T_{\mathrm{c}0}$, i.e. until the superconducting transition temperature in the absence of pseudogap anomalies. At the same time, the superconducting transition temperature T_{c} for a superconductor with a pseudogap is obviously lower than $T_{\mathrm{c}0}$ [63]. Such paradoxical behavior of $\langle\Delta\rangle$ apparently means the appearance of local regions with $\Delta \neq 0$ (superconducting 'drops') in the system, which are induced by fluctuations of D, over the entire temperature range $T_{\mathrm{c}} < T < T_{\mathrm{c}0}$, while a superconducting state coherent over the entire sample occurs only for temperatures below T_{c}. Obviously, analyzing a more realistic model with a finite correlation length ξ of antiferromagnetic short-ranger-order fluctuations is necessary to completely substantiate such a qualitative picture [23]. At the same time, the simplicity of our model with $\xi \to \infty$ makes it possible to immediately arrive at an exact solution for $\langle\Delta\rangle$.

To determine the superconducting transition temperature T_{c} in the sample as a whole we can employ the standard procedure of the mean-field approximation over random short-range-order fluctuations (cf., e.g., a similar approach in the problem of a superconductor with impurities [101]), which implies that the superconducting gap is self-averaging over fluctuations of D (i.e., actually, it is assumed that Δ is independent of fluctuations of D). Then the equations for the mean-field gap Δ_{mf} are

$$1 = \lambda\int_0^{\omega_{\mathrm{c}}} \mathrm{d}\xi \left[\tilde{\alpha}\,\frac{2}{W^2}\int_0^\infty \mathrm{d}D\, D \exp\left(-\frac{D^2}{W^2}\right) \times \frac{\tanh\left(\sqrt{\xi^2 + D^2 + \Delta_{\mathrm{mf}}^2}/2T\right)}{\sqrt{\xi^2 + D^2 + \Delta_{\mathrm{mf}}^2}} + (1-\tilde{\alpha})\,\frac{\tanh\left(\sqrt{\xi^2 + \Delta_{\mathrm{mf}}^2}/2T\right)}{\sqrt{\xi^2 + \Delta_{\mathrm{mf}}^2}}\right] \tag{76}$$

for the case of s-pairing and

$$1 = \lambda\,\frac{4}{\pi}\int_0^{\omega_{\mathrm{c}}} \mathrm{d}\xi \left\{\frac{2}{W^2}\int_0^\infty \mathrm{d}D\, D \exp\left(-\frac{D^2}{W^2}\right) \times \int_0^{\alpha} \mathrm{d}\phi\, e^2(\phi)\,\frac{\tanh\left[\sqrt{\xi^2 + D^2 + \Delta_{\mathrm{mf}}^2 e^2(\phi)}/2T\right]}{\sqrt{\xi^2 + D^2 + \Delta_{\mathrm{mf}}^2 e^2(\phi)}} + \int_{\alpha}^{\pi/4} \mathrm{d}\phi\, e^2(\phi)\,\frac{\tanh\left[\sqrt{\xi^2 + \Delta_{\mathrm{mf}}^2 e^2(\phi)}/2T\right]}{\sqrt{\xi^2 + \Delta_{\mathrm{mf}}^2 e^2(\phi)}}\right\} \tag{77}$$

for the case of d-pairing. These equations represent the limiting form (for $\xi \to \infty$) of the equations for the superconducting gap examined above [Eqn (43)] on the basis of the recurrent procedure (39).

From equations (76) and (77) we can easily obtain the corresponding equations for T_{c}, the temperature at which a gap homogeneous over the sample, Δ_{mf}, emerges. For instance, for the case of s-pairing we have

$$1 = \lambda\left[\tilde{\alpha}\,\frac{2}{W^2}\int_0^\infty \mathrm{d}D\, D \exp\left(-\frac{D^2}{W^2}\right) \times \int_0^{\omega_{\mathrm{c}}} \mathrm{d}\xi\,\frac{\tanh\left(\sqrt{\xi^2 + D^2}/2T_{\mathrm{c}}\right)}{\sqrt{\xi^2 + D^2}} + (1-\tilde{\alpha})\int_0^{\omega_{\mathrm{c}}} \mathrm{d}\xi\,\frac{\tanh(\xi/2T_{\mathrm{c}})}{\xi}\right]. \tag{78}$$

For the case of d-pairing, we must replace $\tilde{\alpha}$ in (78) with the 'effective' α_{d} from (74). These equations for T_{c} coincide with those obtained in the microscopic derivation of the Ginzburg–Landau expansion in Ref. [63] and with the limiting form (for $\xi \to \infty$) that emerges in an analysis based on (39) and (43). In general, we always have $T_{\mathrm{c}\infty} < T_{\mathrm{c}} < T_{\mathrm{c}0}$.

The temperature dependences of the averaged gap $\langle\Delta\rangle$ and the mean-field gap Δ_{mf} obtained through numerical solution of the equations of our model for the case of s-pairing are depicted in Fig. 22a [24]. The gap Δ_{mf} vanishes at $T = T_{\mathrm{c}} < T_{\mathrm{c}0}$, and $\langle\Delta\rangle$ is finite until $T = T_{\mathrm{c}0}$; we believe that the corresponding 'tails' in the temperature dependence of $\langle\Delta\rangle$ for $T_{\mathrm{c}} < T < T_{\mathrm{c}0}$ agree with to the above-mentioned idea of superconducting 'drops' in this temperature range present in the absence of superconductivity in the entire sample. Note that the temperature dependences $\langle\Delta(T)\rangle$ in Fig. 22a resemble the corresponding dependences of the gap in underdoped HTSC cuprates, which can be found from ARPES experiments [49] and specific-heat measurements [19] (see Figs 3 and 11), if we assume that the T_{c} observed in these samples corresponds to our mean-field T_{c}, while 'drops' with $\langle\Delta\rangle \neq 0$ exist even at temperatures higher than T_{c} up to $T_{\mathrm{c}0}$, which is much higher than T_{c}. The fact that the gap is not a self-averaging quantity also manifests itself in our model in that the variance $\langle\Delta^2\rangle - \langle\Delta\rangle^2$ becomes nonzero over the entire temperature range $T < T_{\mathrm{c}0}$, which indirectly supports the proposed qualitative picture, a complete substantiation of which is possible only if one allows for the finiteness of ξ. Note that $T_{\mathrm{c}0}$ is defined rather poorly from the viewpoint of comparisons with experiment. In the above consideration of the transition temperature in the absence of a pseudogap, we assumed that $T_{\mathrm{c}0}$ is of order T_{c} for an optimal carrier

[23] Qualitatively, this situation resembles the onset of an inhomogeneous superconducting state induced by strong fluctuations in the local density of states near the Anderson metal–insulator transition [108, 101].

[24] Qualitatively, the temperature dependences of $\langle\Delta\rangle$ and Δ_{mf} in the case of d-pairing are similar to those in the case of s-pairing.

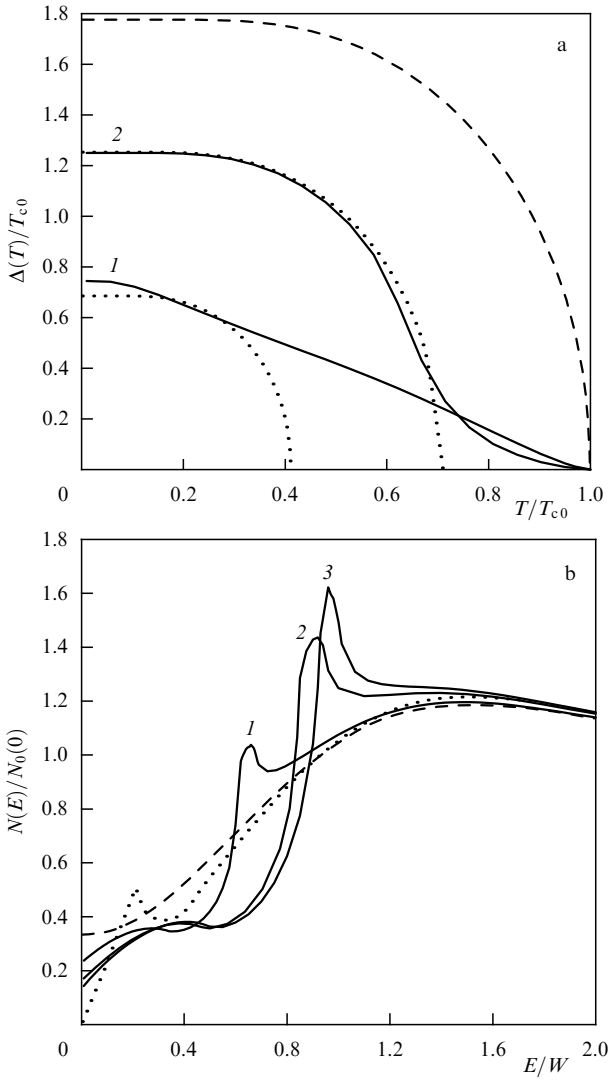

Figure 22. Temperature dependences of the superconducting gaps Δ_{mf} (dotted curves), $\langle\Delta\rangle$ (solid curves), and Δ_0 (dashed curve) in the case of s-pairing [102]: (*1*) $\lambda = 0.4$, $\tilde{\alpha} = 2/3$, and $\omega_c/W = 3$ ($T_c/T_{c0} = 0.42$); (*2*) $\lambda = 0.4$, $\tilde{\alpha} = 0.2$, $\omega_c/W = 1$ ($T_c/T_{c0} = 0.71$). (b) Density of states in the case of d-pairing [102] at $\lambda = 0.4$, $\tilde{\alpha} = 2/3$, and $\omega_c/W = 5$ ($T_c/T_{c0} = 0.48$, with $T_{c\infty}/T_{c0} \sim 10^{-18}$): (*1*) $T/T_{c0} = 0.8$, (*2*) $T/T_{c0} = 0.48$, and (*3*) $T/T_{c0} = 0.1$. The dotted curve represents the behavior of the mean-field density of states $N_{mf}(E)$ at $T/T_{c0} = 0.1$, and the dashed curve represents the pseudogap behavior of the density of states for $T > T_{c0}$.\

concentration. Here, for possible comparisons of the data of Fig. 22a with the data of Figs 3 and 11, the values of T_{c0} must be much higher than the optimal T_c. In this sense, the idea of superconducting 'drops' induced by 'dielectric' fluctuations is not radically different from the ideas used in the scenario of pseudogap formation (precursor pairing). Of course, the data like those presented in Figs 3 and 11 could be a direct implication of the existence of a dielectric pseudogap rather than of the effects of the non-self-averaging nature of the superconducting gap Δ. In particular, the superconducting gap extracted from tunneling data [21, 22] (which manifests itself against the background of a wider pseudogap) demonstrates a 'normal' temperature behavior and vanishes at $T = T_c$.

Although there is no superconductivity in the entire sample for $T_c < T < T_{c0}$, the presence in this temperature range of a nonzero averaged gap $\langle\Delta\rangle$ leads to the appearance of anomalies in the observed quantities, such as the tunneling density of states and the spectral density measured in ARPES experiments [102].

For instance, the tunneling density of states for the case of d-pairing has the form [102]

$$\frac{N(E)}{N_0(0)} = \frac{4}{\pi}\frac{2}{W^2}\int_0^\infty \mathrm{d}D\, D \exp\left(-\frac{D^2}{W^2}\right) \times \left\{\int_0^\alpha \mathrm{d}\phi\, \frac{|E|}{\sqrt{E^2 - D^2 - \Delta^2(D)e^2(\phi)}} \times \theta\left[E^2 - \Delta^2(D)e^2(\phi) - D^2\right] + \int_\alpha^{\pi/4} \mathrm{d}\phi\, \frac{|E|}{\sqrt{E^2 - \Delta^2(D)e^2(\phi)}}\, \theta\left[E^2 - \Delta^2(D)e^2(\phi)\right]\right\}. \quad (79)$$

Under the assumption of self-averaging, Δ equals Δ_{mf} and is independent of D. Then the width of the superconducting pseudogap in the density of states is of order Δ_{mf}, and as $T \to T_c$ the corresponding contribution vanishes, and only the pseudogap related to AFM fluctuations remains. Actually, Δ in (79) is $\Delta(D)$, which can be found from equation (67).

The behavior of the density of states in the d-case is depicted in Fig. 22b. Clearly, there is a substantial difference between the exact density of states and that obtained in the mean-field approximation, and this difference is related to fluctuations of the superconducting gap (superconducting 'drops') caused by antiferromagnetic short-range-order fluctuations. Actually, the exact density of states does not 'feel' the superconducting transition that occurs in the entire system at $T = T_c$; the characteristic width of the superconducting gap (pseudogap) in the density of states is of order Δ_0 rather than Δ_{mf} yielded by the approximation of the mean field over short-range-order fluctuations. The corresponding contributions become observable even at $T = T_{c0} > T_c$.

These results can, at least in principle, explain the unusually large values of the ratio $2\Delta/T_c$ observed in a number of tunnel experiments involving underdoped HTSC cuprates [20, 109] and in ARPES measurements [110]. The presence of superconducting 'drops' in the system can also explain the anomalous diamagnetism of these systems observed in many cases at temperatures higher than T_c [111].

5. Conclusion. Problems and prospects

In conclusion, we sum up the content of this article and examine remaining problems. The scenario of pseudogap formation based on the idea of AFM (SDW or CDW) type short-range-order fluctuations leads to a general qualitative agreement with the basic experimental facts. In our theoretical consideration, we deliberately employed a semi-phenomenological approach based on a simple model of the pseudogap transformation of the electron spectrum, described by two parameters — the effective pseudogap width W and the correlation length ξ, which can be determined (at least in principle) from experiments. The models of 'hot' spots or regions at the Fermi surface, considered here, admit an 'almost exact' solution [14, 15], which makes it possible to achieve a substantial progress in analyzing such problems as the effect of a pseudogap on

superconductivity. Actually, it is unimportant whether we are speaking about AFM fluctuations (as the most popular model) or about short-range-order fluctuations of a different nature that lead to a partial dielectrization of the spectrum, such as CDW or structural distortions.

The drawbacks of these models stem from the simplifying assumptions that are needed to obtained these 'almost exact' solutions. The most important assumptions are the static approximation and the hypothesis of the Gaussian nature of short-range-order fluctuations. Allowance for the dynamics of fluctuation is absolutely necessary in the low-temperature region, in particular, in the superconducting phase, where the pairing interaction itself may be controlled by the dynamics of these fluctuations [58, 59]. We believe, however, that the above simplified consideration can describe the most essential effects of changes in the electron spectrum (pseudogap formation in 'hot' regions of the Fermi surface) and the influence of these changes on superconductivity. To allow for the dynamics of spin fluctuations, we would have to go beyond the simple phenomenology of the BCS model. Also, the assumption of the Gaussian character of the statistics of fluctuations can be justified only at high temperatures and not very close to the line of antiferromagnetic instability. Nevertheless, even in this very simple variant of the model, one can qualitatively describe the basic features of pseudogap formation. The rejection of this very simple assumption also destroys the fairly simple structure of the equations of the theory, which actually makes it possible to analyze the superconducting phase.

We can step beyond the semi-phenomenological approach employed here by means of a complete microscopic analysis of the problem, say, using the Hubbard model. Such attempts have been made by some researchers, e.g., in Refs [11–13] cited above and in Refs [122, 113]. Although many qualitative conclusions of these studies coincide with those discussed here or are close to them, the treatment of the problem is usually limited to allowing for the first few diagrams in perturbation theory [114, 115] or to some variant of self-consistency based on these diagrams. Of course, in this way, one can take into account the dynamics of spin fluctuations. However, going beyond these simple qualitative estimates is fairly difficult.

What would be important is a microscopic justification of the existence of a broad region in the phase diagram with well-developed short-range-order AFM (SDW) fluctuations. Note that the region of such 'critical' fluctuations may be anomalously large simply because of the reduced dimensionality (quasi-two-dimensional structure) of the systems in question. For instance, the size of the region of superconducting fluctuations in HTSC systems is fairly large and can reach tens of kelvins [116]. Since AFM fluctuations are characterized by energies an order of magnitude higher, the presence of a 'critical' region with a width of hundreds of kelvins does not seem unlikely. Nevertheless, there is still no microscopic justification for such a picture.

Apparently, the main qualitative conclusion that can be drawn from the physical picture discussed above concerns the old discussion of whether the spectrum of electronic excitations in HTSC systems is of Fermi-liquid or non-Fermi-liquid nature. According to the simple models examined here, the electron spectrum (spectral density) is of Fermi-liquid nature only in the 'cold' regions of the Fermi surface (near the diagonals of the Brillouin zone), while in the 'hot' regions the spectrum undergoes a non-Fermi-liquid transformation (in the above-specified, narrow sense) due to the strong scattering on AFM fluctuations [14, 15]. The presence or absence of a Fermi-liquid behavior depends on the fluctuation correlation length ξ (cf. [81, 82]). In their recent paper, Abrahams and Varma [117] criticised such a picture on the basic of their fairly successful processing of experimental data [51, 118, 119] for ARPES in optimally doped Bi-2212, using ideas of the theory of marginal Fermi liquids. In particular, Abrahams and Varma [117] state that the decay of quasiparticles does not exhibit Fermi-liquid behavior anywhere on the Fermi surface and also declare that there is no evidence for a momentum dependence of this decay. Actually, however, they introduce a substantial dependence of the static decay on momentum, needed for the description of the data even in the case of optimal doping (under study), which they assign to the anisotropy of impurity scattering. On the other hand, the linear dependence of the decay on the quasiparticle energy, which is actually observed in HTSC systems (and postulated in the theory of marginal Fermi liquids), cannot serve as a refutation of the ordinary ideas of the Fermi-liquid theory, since a standard quadratic dependence can be observed only in a fairly narrow energy interval near the Fermi level that is beyond the limit of accuracy of ARPES experiments. An exhaustive discussion of these aspects can be found in reviews by Maksimov [91] and Ginzburg and Maksimov [93]. Generally, it should be noted that the presence of anomalous scattering on AFM fluctuations (with wave vectors of order of the antiferromagnetism vector) is beyond question [25].

Our theoretical consideration was based on the fairly traditional scheme of averaging over the mean field of AFM (SDW, CDW) fluctuations, which assumes the spatial homogeneity of the system on average. At the same time, some experimental data and theoretical ideas point to the possibility of phase separation in a number of HTSC systems (especially in the region of underdoped compositions) [121, 122]. Such separation occurs on a microscopic scale, so that the system separates into 'metallic' (superconducting) and 'dielectric' (antiferromagnetic) domains with characteristic sizes of order of several interatomic distances. Naturally, it is rather difficult to describe such a system using the above standard methods, while the very fact of phase separation may play, as many researchers believe, a crucial role in HTSC physics. In this context we only remark that the qualitative picture of the random field of AFM (SDW, CDW) short-range-order fluctuations, used above, also indirectly assumes the appearance of effective regions with AFM order in the system, of a characteristic size $\sim \xi$, that alternate with regions of the same size in which this order is destroyed. In this sense our picture does not strongly differ from the pattern of phase separation — the only difference is probably in that the boundaries of the corresponding regions are diffuse. Clearly the formalism of some models of phase separation based on the idea of proximity to a CDW-type instability [64, 123, 124] is fairly close to that used in this review and is based on the picture of scattering on fluctuations with some distinguished wave vectors.

[25] We would like to mention the interesting work done by Li Jian-Xin et al. [120], who managed to give a fairly good description of the kinetic properties of HTSC oxides on the basis of a simple consideration of Boltzmann scattering on spin fluctuations with a straightforward elimination of the contributions from 'hot' regions of the Fermi surface to the current-carrier kinetics.

Finally, it is worth noting that HTSC systems contain a large number of anomalies related to the behavior of such systems under sufficiently strong structural disordering [101]. The role of structural disordering in systems with a pseudogap is understood very poorly. There are only a few papers that examine the effect of substitutional impurities [125, 126]. They show that controlled disordering can serve as a fairly informative method of studying the pseudogap state. This problem has not yet been studied theoretically almost at all.

The study of anomalies in HTSC systems related to pseudogap formation is of considerable importance for applications. Since, as we have seen, the pseudogap suppresses, in a certain sense, superconductivity, such characteristics of a superconductor as the critical current and the critical magnetic fields prove to be maximum not at the 'optimal' carrier concentration $p_0 \sim 0.15-0.17$ corresponding to the maximum T_c but in the vicinity of the 'critical' concentration $p_c \approx 0.19$ [127]. This fact may be important for optimizing the compositions of commercial HTSC-type superconductors.

I am grateful to É Z Kuchinskiĭ, my coworker in a number of the most important studies, which were used in the theoretical section of this review.

The work was supported in part by the Russian Foundation for Basic Research (Grant No. 99-02-16285) and CRDF (Grant No. REC-005), the State Programs in Statistical Physics (Grant No. 108-11(00)-P) and High-T_c Superconductivity (Grant No. 96-051), and the Quantum Microphysics Program of Basic Research of the Presidium of the Russian Academy of Sciences.

References

1. Batlogg B, Varma C *Phys. World* **13** 33 (2000)
2. Timusk T, Statt B *Rep. Prog. Phys.* **62** 61 (1999)
3. Randeria M, in *Varenna Lectures 1997*; cond-mat/9710223
4. Randeria M, Campuzano J-C, in *Varenna Lectures 1997*; cond-mat/9709107
5. Tohyama T, Maekawa S *Supercond. Sci. Tech.* **13** R17 (2000); cond-mat/0002225
6. Tallon J L, Loram J W *Physica C* **349** 53 (2001); cond-mat/0005063
7. Geshkenbein V B, Ioffe L B, Larkin A I *Phys. Rev. B* **55** 3173 (1997)
8. Emery V, Kivelson S A, Zachar O *Phys. Rev. B* **56** 6120 (1997)
9. Maly J, Janko B, Levin K *Phys. Rev. B* **56** R11407 (1997); **59** 1354 (1999); cond-mat/9710187, 9805018
10. Gusynin V P, Loktev V M, Sharapov S G *Zh. Eksp. Teor. Fiz.* **115** 1243 (1999) [*JETP* **88** 685 (1999)]
11. Kampf A P, Schrieffer J R *Phys. Rev. B* **41** 6399 (1990); **42** 7967 (1990)
12. Langer M et al. *Phys. Rev. Lett.* **75** 4508 (1995)
13. Deisz J J, Hess D W, Serene J W *Phys. Rev. Lett.* **76** 1312 (1996)
14. Schmalian J, Pines D, Stojkovic B *Phys. Rev. Lett.* **80** 3839 (1998); *Phys. Rev. B* **60** 667 (1999)
15. Kuchinskiĭ É Z, Sadovskiĭ M V *Zh. Eksp. Teor. Fiz.* **115** 1765 (1999) [*JETP* **88** 968 (1999)]; cond-mat/9808321
16. Chakravarty S et al., cond-mat/0005443
17. Mott N F, Davis E A *Electronic Processes in Non-Crystalline Materials* (Oxford: Clarendon Press, 1971) [Translated into Russian (Moscow: Mir, 1974)]
18. Loram J W et al. *Physica C* **282–287** 1405 (1997)
19. Loram J W et al. *J. Supercond.* **7** 243 (1994)
20. Renner C et al. *Phys. Rev. Lett.* **80** 149 (1998)
21. Krasnov V M et al. *Phys. Rev. Lett.* **84** 5860 (2000)
22. Krasnov V M et al. *Phys. Rev. Lett.* **86** 2657 (2001); cond-mat/0006479
23. Bucher B et al. *Phys. Rev. Lett.* **70** 2021 (1993)
24. Yasuoka H *Hyperfine Interact.* **105** 27 (1997)
25. Alloul H, Adrian F J *Phys. Rev. Lett.* **63** 1700 (1989)
26. Gorny K et al. *Phys. Rev. Lett.* **82** 177 (1999); cond-mat/9812013
27. Zheng G-Q et al. *Phys. Rev. Lett.* **85** 405 (2000)
28. Tallon J L et al. *Phys. Status Solidi B* **215** 531 (1999); cond-mat/9911157
29. Puchkov A V, Basov D N, Timusk T *J. Phys.: Condens. Matter* **8** 10049 (1996)
30. Startseva T et al. *Phys. Rev. B* **59** 7184 (1999)
31. Dessau D S et al. *Phys. Rev. Lett.* **71** 2781 (1993)
32. Shen Z X, Dessau D S *Phys. Rep.* **253** 1 (1995)
33. Ino A et al. *J. Phys. Soc. Jpn.* **68** 1496 (1999); cond-mat/9809311
34. Gatt R et al., cond-mat/9906070
35. Feng D L et al., cond-mat/9908056
36. Chuang Y D et al. *Phys. Rev. Lett.* **83** 3717 (1999)
37. Gromko A D et al., cond-mat/0003017
38. Bogdanov P V et al., cond-mat/0005394
39. Fretwell H M et al. *Phys. Rev. Lett.* **84** 4449 (2000)
40. Mesot J et al., cond-mat/9910430
41. Bansil A et al. *Phys. Rev. Lett.* **83** 5154 (1999)
42. Borisenko S V et al. *Phys. Rev. Lett.* **84** 4453 (2000)
43. Legner S et al. *Phys. Rev. B* **62** 154 (2000); cond-mat/0002302
44. Norman M R et al., cond-mat/9710163
45. Annett J, Goldenfeld N, Leggett A, in *Physical Properties of High Temperature Superconductors* Vol. 5 (Ed. D M Ginsberg) (Singapore: World Scientific, 1996) p. 375; cond-mat/9601060
46. Izyumov Yu A *Usp. Fiz. Nauk* **169** 225 (1999) [*Phys. Usp.* **42** 215 (1999)]
47. Tsuei C C, Kirtley J R *Rev. Mod. Phys.* **72** 969 (2000)
48. Ding H et al. *Nature* **382** 51 (1996)
49. Norman M R et al. *Nature* **392** 157 (1998)
50. Norman M R et al. *Phys. Rev. B* **57** R11093 (1998)
51. Kaminski A et al. *Phys. Rev. Lett.* **84** 1788 (2000); cond-mat/9904390
52. Ronning F et al. *Science* **282** 2067 (1998); cond-mat/9903151
53. Hackl R, in *The Gap Symmetry and Fluctuations in High-T_c Superconductors* (Eds J Bok, G Deutscher, D Pavuna) (New York: Plenum Press, 1998) p. 249
54. Bourges P, in *The Gap Symmetry and Fluctuations in High-T_c Superconductors* (Eds J Bok, G Deutscher, D Pavuna) (New York: Plenum Press, 1998) p. 349
55. Schrieffer J R, Wen X G, Zhang S C *Phys. Rev. B* **39** 11663 (1989)
56. Izyumov Yu A *Usp. Fiz. Nauk* **161** (11) 1 (1991) [*Sov. Phys. Usp.* **34** 935 (1991)]
57. Ziman J M *Principles of the Theory of Solids* 2nd ed. (Cambridge: The Univ. Press, 1972) [Translated into Russian (Moscow: Mir, 1974)]
58. Monthoux P, Balatsky A V, Pines D *Phys. Rev. B* **46** 14803 (1992)
59. Monthoux P, Pines D *Phys. Rev. B* **47** 6069 (1993); **49** 4261 (1994)
60. Millis A J, Monien H, Pines D *Phys. Rev. B* **42** 167 (1990)
61. Barzykin V, Pines D *Phys. Rev. B* **52** 13585 (1995)
62. Pines D *Z. Phys. B* **103** 129 (1997)
63. Posazhennikova A I, Sadovskiĭ M V *Zh. Eksp. Teor. Fiz.* **115** 632 (1999) [*JETP* **88** 347 (1999)]
64. Benfatto L, Caprara S, Di Castro C *Eur. J. Phys. B* **71** 95 (2000)
65. Virosztek A, Ruvalds J *Phys. Rev. B* **42** 4064 (1990)
66. Ruvalds J et al. *Phys. Rev. B* **51** 3797 (1995)
67. Zheleznyak A T, Yakovenko V M, Dzyaloshinskii I E *Phys. Rev.* **55** 3200 (1997)
68. Ziman J M *Models of Disorder* (Cambridge: Cambridge Univ. Press, 1979) [Translated into Russian (Moscow: Mir, 1982)]
69. Abrikosov A A, Gor'kov L P, Dzyaloshinskiĭ I E *Metody Kvantovoĭ Teorii Polya v Statisticheskoĭ Fizike* (Quantum Field Theoretical Methods in Statistical Physics) (Moscow: Fizmatgiz, 1962) [Translated into English (Oxford: Pergamon Press, 1965)]
70. Lee P A, Rice T M, Anderson P W *Phys. Rev. Lett.* **31** 462 (1973)
71. Sadovskiĭ M V *Zh. Eksp. Teor. Fiz.* **66** 1720 (1974) [*Sov. Phys. JETP* **39** 845 (1974)]
72. Sadovskiĭ M V *Fiz. Tverd. Tela* (Leningrad) **16** 2504 (1974) [*Sov. Phys. Solid State* **16** 1632 (1974)]
73. Sadovskiĭ M V *Zh. Eksp. Teor. Fiz.* **77** 2070 (1979) [*Sov. Phys. JETP* **50** 989 (1979)]
74. Elyutin P V *Opt. Spektrosk.* **43** 542 (1977) [*Opt. Spectrosc.* **43** 318 (1977)]
75. Tchernyshyov O *Phys. Rev. B* **59** 1358 (1999)
76. Sadovskii M V *Physica C* **341–348** 811 (2000)

77. Bartosh L, Kopietz P *Phys. Rev. B* **60** 15488 (1999)
78. Millis A J, Monien H *Phys. Rev. B* **61** 12496 (2000)
79. Marshall D S et al. *Phys. Rev. Lett.* **76** 4841 (1996)
80. Sadovskiĭ M V, Timofeev A A *Sverkhprovodimost'*: *Fiz. Khim. Tekhnol.* **4** (1) 11 (1991) [*Superconductivity*: *Phys. Chem. Technol.* **4** 9 (1991)]; Sadovskii M V, Timofeev A A *Physica C* **185–189** 1431 (1991)
81. Sadovskii M V, Timofeev A A *J. Moscow Phys. Soc.* **1** 391 (1991)
82. McKenzie R H, Scarratt D *Phys. Rev. B* **54** R12709 (1996)
83. Sadovskiĭ M V *Pis'ma Zh. Eksp. Teor. Fiz.* **69** 447 (1999) [*JETP Lett.* **69** 483 (1999)]; *Physica C* **341–348** 939 (2000); cond-mat/9902192
84. Puchkov A V et al. *Phys. Rev. Lett.* **77** 3212 (1996)
85. Basov D N et al. *Phys. Rev. Lett.* **77** 4090 (1996)
86. Strigina N A, Diploma Thesis (Ekaterinburg: Ural State Univ., 2001)
87. Abanov Ar, Chubukov A V, Finkel'stein A M, cond-mat/9911445
88. Abanov Ar, Chubukov A V, cond-mat/0002122
89. Abanov Ar, Chubukov A V, Schmalian J, cond-mat/0005163
90. Abanov Ar, Chubukov A V, Schmalian J, cond-mat/0010403
91. Maksimov E G *Usp. Fiz. Nauk* **170** 1033 (2000) [*Phys. Usp.* **43** 965 (2000)]
92. Kulić M *Phys. Rep.* **338** 1 (2000)
93. Ginzburg V L, Maksimov E G *Sverkhprovodimost'*: *Fiz. Khim. Tekhnol.* **5** 1543 (1992) [*Superconductivity*: *Phys. Chem. Technol.* **5** 1505 (1992)]
94. Friedel J, Kohmoto M, cond-mat/9901065
95. Anderson P W *The Theory of Superconductivity in the High-T_c Cuprates* (Princeton, N.J.: Princeton Univ. Press, 1997)
96. Borkowski L S, Hirschfeld P J *Phys. Rev. B* **49** 15404 (1994)
97. Fehrenbacher R, Norman M R *Phys. Rev. B* **50** 3495 (1994)
98. Kuchinskiĭ É Z, Sadovskiĭ M V *Zh. Eksp. Teor. Fiz.* **119** 553 (2001) [*JETP* **92** 480 (2001)]
99. Gor'kov L P *Zh. Eksp. Teor. Fiz.* **37** 1407 (1959) [*Sov. Phys. JETP* **10** 998 (1960)]
100. de Gennes P G *Superconductivity of Metals and Alloys* (New York: W A Benjamin, 1966) [Translated into Russian (Moscow: Mir, 1968)]
101. Sadovskii M V *Superconductivity and Localization* (Singapore: World Scientific, 2000); *Phys. Rep.* **282** 225 (1997); *Sverkhprovodimost'*: *Fiz. Khim. Tekhnol.* **8** 337 (1995)
102. Kuchinskiĭ É Z, Sadovskiĭ M V *Zh. Eksp. Teor. Fiz.* **117** 613 (2000) [*JETP* **90** 535 (2000)]; *Physica C* **341–348** 879 (2000)
103. Balatsky A V, Bourges P *Phys. Rev. Lett.* **82** 5337 (1999)
104. Tallon J L, cond-mat/9911422
105. Kopaev Yu V *Tr. Fiz. Inst. Akad. Nauk SSSR* **86** 3 (1975) [*Proc. Lebedev Phys. Inst.* Vol. 86 (New York: Plenum Press, 1977) p. 1]
106. Ginzburg V L, Kirzhnits D A (Eds) *Problema Vysokotemperaturnoĭ Sverkhprovodimosti* (The Problem of High-Temperature Superconductivity) Chap. 5 (Moscow: Nauka, 1977) p. 205 [Translated into English: *High-Temperature Superconductivity* (New York: Consultants Bureau, 1982)]
107. Bilbro G, McMillan W L *Phys. Rev. B* **14** 1887 (1976)
108. Bulaevskiĭ L N, Panyukov S V, Sadovskiĭ M V *Zh. Eksp. Teor. Fiz.* **92** 672 (1987) [*Sov. Phys. JETP* **65** 380 (1987)]
109. Miyakawa N et al. *Phys. Rev. Lett.* **80** 157 (1998)
110. Harris J M et al. *Phys. Rev. B* **54** R15665 (1996)
111. Carretta P et al., cond-mat/9911182
112. Schmalian J et al. *Phys. Rev. B* **54** 4336 (1996)
113. Vilk Y M, Tremblay A-M S *J. Phys. I* (Paris) **7** 1309 (1997)
114. Vilk Y M *Phys. Rev. B* **55** 3870 (1997)
115. Monthoux P *Phys. Rev. B* **55** 11111 (1997)
116. Junod A, Erb A, Renner C *Physica C* **317–318** 333 (1999)
117. Abrahams E, Varma C M, cond-mat/0003135; submitted to *Proc. Natl. Acad. Sci.*
118. Valla T et al. *Science* **285** 2110 (1999)
119. Valla T et al. *Phys. Rev. Lett.* **85** 828 (2000); cond-mat/0003407
120. Li Jian-Xin, Wu W C, Lee T K *Phys. Rev. B* **60** 3629 (1999); cond-mat/9901322
121. Nagaev É L *Usp. Fiz. Nauk* **165** 529 (1995) [*Phys. Usp.* **38** 497 (1995)]
122. Zaanen J *Physica C* **317–318** 217 (1999)
123. Castellani C, Di Castro C, Grilli M *Phys. Rev. Lett.* **75** 4650 (1995)
124. Caprara S et al. *Physica C* **317–318** 230 (1999)
125. Tallon J L et al. *Phys. Rev. Lett.* **79** 5294 (1997)
126. Tallon J L *Phys. Rev. B* **58** R5956 (1998)
127. Tallon J L, Williams G V M, Loram J W *Physica C* **338** 9 (2000)